

# Distribution of auxin and PIN proteins during somatic embryogenesis of *Brachypodium distachyon*

---

Lelas, Luka

Master's thesis / Diplomski rad

2022

Degree Grantor / Ustanova koja je dodijelila akademski / stručni stupanj: **University of Zagreb, Faculty of Science / Sveučilište u Zagrebu, Prirodoslovno-matematički fakultet**

Permanent link / Trajna poveznica: <https://um.nsk.hr/um:nbn:hr:217:010033>

Rights / Prava: [In copyright](#) / [Zaštićeno autorskim pravom.](#)

Download date / Datum preuzimanja: **2025-03-29**



Repository / Repozitorij:

[Repository of the Faculty of Science - University of Zagreb](#)



University of Zagreb  
Faculty of Science  
Department of Biology

Luka Lelas

**Distribution of auxin and PIN proteins  
during somatic embryogenesis of  
*Brachypodium distachyon***

Master thesis

Zagreb, 2022.

Sveučilište u Zagrebu  
Prirodoslovno-matematički fakultet  
Biološki odsjek

Luka Lelas

**Lokalizacija auksina i proteina PIN  
tijekom somatske embriogeneze vrste  
*Brachypodium distachyon***

Diplomski rad

Zagreb, 2022.

This thesis was created in the research team Cell Biology and Plant Regeneration of the Institut Jean-Pierre Bourgin, INRAE at Versailles, under supervision of dr. sc. Oumaya Bouchabké-Coussa and under co-mentorship of prof. dr. sc. Dunja Leĳak Levanić. The thesis was presented for evaluation to the Department of Biology, Faculty of Science, Zagreb for acquiring the title of Master in Molecular Biology.

First of all, I would like to express my gratitude to Pierre and Oumaya for accepting me in their team and for being patient and understanding mentors. My appreciation goes especially to Oumaya for being the best supervisor one could ask for. Next, I owe substantial gratitude to professor Leljak-Levanić, for her essential advice on writing and helping me bring this work to completion. Last but not least, I would like to thank my family for supporting me through my education. Final thank you goes to Klara, who always supported and motivated me.

# TEMELJNA DOKUMENTACIJSKA KARTICA

---

Sveučilište u Zagrebu  
Prirodoslovno-matematički fakultet  
Biološki odsjek

Diplomski rad

## Lokalizacija auksina i proteina PIN tijekom somatske embriogeneze te regeneracije vrste *Brachypodium distachyon*

Luka Lelas

Rooseveltove trg 6, 10000 Zagreb, Hrvatska

*Brachypodium distachyon* je vrsta koja se koristi pri proučavanju porodice *Poaceae*. Njena filogenetska povezanost s jednosupnicama od agronomske važnosti čini je idealnom za proučavanje razvojnih mehanizama s ekonomskim primjenama, poput somatske embriogeneze (SE). Kako auksin ima ključnu ulogu u SE, praćenje njegove prisutnosti tijekom SE omogućava opisivanje tog procesa u cjelini. U tu svrhu, odabrani su fluorescentno označeni transporteri auksina PIN-FORMED (PIN) za prisutnost auksina te proučeni pomoću konfokalnog mikroskopa ili konfokalne mikroskopije. Rezultati su pokazali da je PIN1a važan marker SE budući da je eksprimiran tijekom svih stadija SE te da su obrasci distribucije SoPIN1 i PIN1b komplementarni i međusobno isključivi. Štoviše, proučavanje markera prisutnosti auksina pokazalo je na koji način SoPIN1 i PIN1b utječu na njegov tok i time oblikuju SE. Uz navedeno je proučen učinak odabranih PIN auksinskih transportera na proces SE, uspoređujući odgovor loss-of-function mutanta *pin1a*, *pin1b* te njihovog križanca *pin1a* × *pin1b* na indukciju SE *in vitro* koristeći se bojanjem PAS/NBB. Histološke razlike mutanata i eksplantanata divljeg tipa nisu utvrđene, što ukazuje kako funkcionalna redundantnost preostalih proteina PIN omogućava odvijanje SE.

Ključne riječi: *Brachypodium*, *in vitro* uzgoj, somatska embriogeneza, konfokalna mikroskopija

(70 stranica, 11 slika, 4 tablice, 64 literaturnih navoda, jezik izvornika: engleski)

Rad je pohranjen u Središnjoj biološkoj knjižnici

Mentor: dr. sc. Oumaya Bouchabké-Coussa

Komentor: prof. dr. sc. Dunja Leljak-Levanić

Ocjenitelji:

prof. dr. sc. Dunja Leljak-Levanić

prof. dr. sc. Željka Vidaković-Cifrek

izv. prof. dr. sc. Petra Peharec Štefanić

Rad prihvaćen: 8.12.2022.

## BASIC DOCUMENTATION CARD

---

University of Zagreb  
Faculty of Science  
Department of Biology

Master thesis

### Distribution of auxin and PIN proteins during somatic embryogenesis and regeneration of *Brachypodium distachyon*

Luka Lelas

Rooseveltova trg 6, 10000 Zagreb, Croatia

*Brachypodium distachyon* is a model species used for research of *Poaceae*. The phylogenetic link this species shares with monocots of agronomic importance makes it the ideal model for studying developmental mechanism with economic applications, like somatic embryogenesis (SE). As auxin plays a critical role in SE, tracking its presence during SE enables description of the process as a whole. For this purpose, fluorescently-tagged PIN-FORMED (PIN) auxin transporters and presence of auxin was examined using confocal microscopy. Findings confirmed PIN1a to be a major marker of SE as it is expressed in all stages of SE and revealed the complementary but mutually exclusive distribution patterns of SoPIN1 and PIN1b. Moreover, examinations of markers of auxin presence revealed how SoPIN1 and PIN1b affect its flow and thus influence SE. Additionally, with the goal of furthering understanding of the effect these select PIN auxin transporters have on SE, response of loss-of-function mutants *pin1a*, *pin1b* and their cross *pin1a* × *pin1b* to *in vitro* SE induction was compared using PAS/NBB staining. Results have shown no identifiable histological differences in comparison to wild-type explants, hinting at functional redundancy of the remaining PIN transporters allowing SE to occur.

Keywords: *Brachypodium*, *in vitro* culture, somatic embryogenesis, confocal microscopy (70 pages, 11 figures, 4 tables, 64 references, original work in: English)  
Thesis is deposited in Central Biological Library.

Mentor: dr. sc. Oumaya Bouchabké-Coussa  
Co-mentor: prof. dr. sc. Dunja Leljak-Levanić

#### Reviewers:

prof. dr. sc. Dunja Leljak-Levanić  
prof. dr. sc. Željka Vidaković-Cifrek  
izv. prof. dr. sc. Petra Peharec Štefanić

Thesis accepted: 8.12.2022.

## Table of Contents

---

1. INTRODUCTION .....	1
1.1 Somatic embryogenesis .....	1
1.1.1 General introduction .....	1
1.1.2 Somatic versus zygotic embryogenesis .....	2
1.1.3 Main aspects of somatic embryogenesis induction .....	3
1.1.4 Somatic embryogenesis in monocotyledons .....	6
1.1.5 Applications of somatic embryogenesis .....	6
1.2. Monocotyledonous model species <i>Brachypodium distachyon</i> .....	8
1.2.1. General introduction .....	8
1.2.2 Somatic embryogenesis in <i>Brachypodium distachyon</i> .....	10
1.3 Effects and control of auxin in plant development .....	15
1.3.1 Physiological role of auxin.....	15
1.3.2 Molecular recognition of auxin .....	16
1.3.3 Polar auxin transport.....	17
1.3.4 PIN-FORMED auxin transporters.....	19
1.3.5 PIN-FORMED auxin transporters in monocotyledons.....	20
1.3.6 PIN-FORMED auxin transporters in <i>B. distachyon</i> .....	21
1.3.7 Experimental methods for tracking auxin .....	23
2. AIM OF RESEARCH.....	26
3. MATERIALS AND METHODS .....	27
3.1 Materials .....	27
3.1.1 Plant material.....	27
3.1.2 Greenhouse cultivation substrate.....	28
3.1.3 Plant nutrition media.....	28
3.2 Methods .....	29
3.2.1 Greenhouse cultivation of plant material .....	29
3.2.2 Harvesting and sterilization of plant material .....	30
3.2.3 Isolation of immature zygotic embryos .....	30
3.2.4 Somatic embryogenesis induction .....	30
3.2.5 Preparation of fluorescent tag-carrying explants for confocal microscopy .....	31
3.2.6 Microtome section preparation for staining of loss-of-function mutants .....	32



3.2.7 Staining of loss-of-function mutant tissue sections .....	33
3.2.8 Confocal microscopy .....	33
3.2.9 Bright-field microscopy .....	34
4. RESULTS .....	36
4.1. Distribution of PIN1a during somatic embryogenesis .....	36
4.2 Distribution of PIN1b, SoPIN1 and the transcriptional response to auxin during somatic embryogenesis .....	39
4.3 Presence of auxin tracked with the DII-VENUS during somatic embryogenesis .....	44
4.4 Comparison of tissue sections of <i>B. distachyon pin</i> loss-of-function mutant explants undergoing somatic embryogenesis .....	46
5. DISCUSSION .....	50
5.1 Occurrence of PIN1a in somatic embryogenesis of <i>B. distachyon</i> .....	50
5.2 Occurrence of PIN1b and SoPIN1 in somatic embryogenesis of <i>B. distachyon</i> .....	52
5.3 The occurrence and flow of auxin during somatic embryogenesis of <i>B. distachyon</i> .....	54
5.4 Histological traits of PAS/NBB stained loss-of-function mutants <i>pin1a</i> , <i>pin1b</i> and <i>pin1a</i> × <i>pin1b</i> of <i>B. distachyon</i> .....	57
5.5 Proposed hypothetical model of developmental events occurring during somatic embryogenesis of <i>B. distachyon</i> .....	59
6. CONCLUSION .....	62
7. REFERENCES .....	64
8. CURRICULUM VITAE .....	70
9. APPENDIX .....	I
9.1 Distribution of PIN1a during somatic embryogenesis .....	I
9.2 Distribution of PIN1b, SoPIN1 and the transcriptional response to auxin during somatic embryogenesis .....	II
9.3 Comparison of tissue sections of <i>B. distachyon pin</i> loss-of-function mutant explants not responding to somatic embryogenesis .....	V

## Abbreviations

2,4-D - 2,4-dichlorophenoxyacetic acid

CIM - Callus-induction medium

D0<sub>CIM</sub> – explant stage before placement on CIM

D1<sub>CIM</sub> – stage reached by the explant after 24 hours on CIM

D1<sub>SIM</sub> - stage reached by the explant after 72 hours on CIM and 24 hours on SIM

D2<sub>CIM</sub> - stage reached by the explant after 48 hours on CIM

D2<sub>SIM</sub> - stage reached by the explant after 72 hours on CIM and 48 hours on SIM

D3<sub>CIM</sub> - stage reached by the explant after 72 hours on CIM

D3<sub>SIM</sub> - stage reached by the explant after 72 hours on CIM and 72 hours on SIM

IAA - Indole acetic acid

ISH – *in situ* hybridization

PAT - Polar auxin transport

PIN - PIN-FORMED auxin transporter protein

SE - Somatic embryogenesis

sEMBs - Somatic embryos

SIM - Shoot-induction medium

zEMBs - Zygotic embryos

# 1. INTRODUCTION

---

## 1.1 Somatic embryogenesis

### 1.1.1 General introduction

Somatic embryogenesis (SE) is a developmental process enabled by the inherent genetic plasticity of the plant kingdom. In its essence, it is a pathway through which somatic embryos (sEMBs) are generated from developmentally-determined vegetative cells. Overriding the developmental fate of these cells through *in vitro* manipulation creates a biotechnological tool whose capabilities allow advancements in research and applications in agrotechnology.

The study of SE dates back to the early 20<sup>th</sup> century, when the father of plant physiology Gottlieb Haberlandt first discussed the idea of cell growth, division, totipotency and differentiation in his *Physiologische Pflanzenanatomie* published in 1924. His understanding of the nature of cells lead him to theorize that by growing isolated cells and encouraging their differentiation, deductions could be made on factors affecting development of plant tissues. Although he was not able to progress far, he laid the conceptual foundation of the field of plant *in vitro* cultivation, which eventually lead to discovery of SE (Kutschera & Ray 2021).

First observations of SE occurring naturally were made in the genus *Kalanchoë* during the 1930s. Species of this genus develop propagules on the edges of their leaves, be it constitutively or through environmental stress. Significant breakthrough in the field came in the second half of the 20<sup>th</sup> century, partly due to introduction of aseptic culturing methods. In the final years of the 1950s, first observations on induced sEMB formation during *in vitro* culturing of various plant species were made (reviewed by Kutschera & Ray 2021). This research caught on the general academic community in the 1960s and from then, the advancements in SE are continuously being made to this day. The list of species SE has been induced in has grown rapidly with protocol optimization and with the advent of molecular biology at the end of the century, the field of SE is starting to shift from empiricism to a more analytical approach (Loyola-Vargas & Ochoa-Alejo 2016).

Today, *Arabidopsis thaliana* (L.) Heynh stands as the principal model system for SE studies but the need arises for study of other systems, ones which would yield knowledge more relatable to species of economic importance, be it crops, species of pharmaceutical significance or endangered species.

### 1.1.2 Somatic versus zygotic embryogenesis

The existence of another embryo-yielding pathway, different to the one responsible for zygotic embryogenesis, begs the question on their commonalities and differences. In general, embryos of both origins share morphological features but differ most substantially both in initial and final stages of their developmental fate. The morphological similarities were established early, with Zimmerman (1993) observing that, among other aspects, sEMBs resemble their zygotic counterparts during development, both morphologically and temporally.

While sEMBs usually arise from vegetative cells following *in vitro* manipulations, zygotic embryos (zEMBs) are created as the ultimate product of sexual reproduction through fusion of the haploid female egg cell and male sperm cell. In *Arabidopsis*, first division of the zygote gives rise to a bipolar two-cell embryo from which all the lineages that form the later embryological stages come to existence. The zygote is surrounded and nurtured by the maternal tissues, which continues until maturation of the complete seed (Leljak-Levanić et al. 2015). Somatic embryos, on the other hand, develop either from somatic cells that kept their pluripotent potential or from cells that first dedifferentiated back to a totipotent state. Whether they are derived from one or multiple cells is not entirely resolved, but in many SE systems the so-called proembryogenic masses predate the appearance of larger structures. These proembryogenic masses are identified as clusters of small, cytoplasm rich embryogenic cells (Winkelman 2016). The main problem of identifying their origin is the difficulty of pin-pointing the often inconspicuous cell or group of cells that they arise from, so the true origin of sEMBs remains obscure.

The study performed by Jin et al. (2013) is a rare review of comparative transcriptomics of the two types of embryos. It offers insight into the shared genetic aspects that point to similar gene sets being responsible for both pathways of embryogenesis. Studying the transcriptomic profiles of somatic and zygotic cotton embryos, they found that these explants share 38% of differentially expressed genes during the globular and up to 51% at the cotyledonal stage. The shared genes have functions in basic cellular metabolic and developmental processes, stimuli response, biological regulation and cellular component organization while the differing ones are connected mostly to stress-response genes, an important aspect of *in vitro* induction of SE.

Also, while sharing the post-initial aspects of embryo development, the two types of embryos differ in their relation to their surroundings, as in the final stage of development. In parallel to the growth of the zEMB, the endosperm proliferates and goes through cellularization,

surrounding and nourishing the embryo throughout its growth and maturation. sEMBs lack this connection to the maternal tissues and are not embedded into the endosperm, instead taking-up nutrients from their surroundings. As a way of offsetting the harsh conditions that come along with growth in an artificial environment, callose deposition and modifications of cell surface have been implicated as a defense mechanisms employed by sEMBs. Callose deposition is not only a physiological reaction destined for minimizing abiotic stress on a tissue level, but it possibly contributes to creation of carbohydrate and protein reserves along with establishing morphogenetic patterns through cell isolation (Leljak-Levanić et al. 2015). As for the modifications of the cell wall, it is suspected that they have a role in morphogenesis by regulation of intercellular communication (Leljak-Levanić et al. 2015). Overall, as Winkelmann (2016) sums up, sEMBs are generally more exposed to stress than their zygotic counterparts; they accumulate less storage compounds and do not undergo a proper maturation phase which includes growth arrest, as they rather germinate immediately after formation.

### 1.1.3 Main aspects of somatic embryogenesis induction

Two developmental routes can be followed when inducing SE, known as the indirect and the direct pathway (Horstman et al. 2017). The indirect pathway's main feature is the phase of callogenesis that results in callus tissue from which proembryogenic masses (PEMs) and their derivatives, somatic embryos, form. The common conception about callus is that it contains both undifferentiated and differentiated cell types, but these notions are being questioned through novel research. Horstman et al. (2017) points to discoveries concerning molecular level examinations that shed light on the nature of callus tissue. Researchers detected the similarity in *A. thaliana* callus gene expression to root meristem expression (Sugimoto et al. 2010), tracked *A. thaliana* callus origin to the pericycle-related cells of root and aerial organs and discovered similarities in callus development to lateral root formation pathways (Atta et al. 2009). Such findings gradually bring to light the developmental and molecular mechanism governing SE, especially because majority of protocols (Wójcikowska & Gaj 2016) utilize the indirect pathway for induction due to better suitability of callus tissues for induction and regeneration in a liquid culturing medium.

The direct pathway of SE is generally less studied and utilized. As its name implies, no callus tissue develops from the explant undergoing direct induction and the sEMB originates from the tissues of the explant itself. Williams & Maheswaran (1986) describe the sequence of events that result in direct formation of sEMBs as first starting with divisions of one or multiple cell layers that lead to bulging of the epidermal surface and from these protrusions sEMBs

gradually develop. The cells which start the bulging process have not been identified to this day, as mentioned previously.

Understanding the factors influencing SE induction *in vitro* is of major interest when considering the many applications of this process. To highlight the principal elements governing it, a common workflow protocol of induction in *A. thaliana*, based on the survey of 17 protocols reviewed by Wójcikowska & Gaj (2016), is presented.

The starting explant material defines the callogenic and embryogenic potential and thus most of the protocols use the immature zygotic embryos isolated 11 to 13 days after pollination as other tissues hardly compare to their 90% induction rate. Post-embryonic tissues such as seeds, germinating seeds, seedlings, 5-week-old roots, hypocotyls and cotyledons of 6-day-old seedlings or leaf mesophyll from 3- to 4-week old plants are also susceptible to SE induction, but their induction efficiency is in the range of 0 to 50% (Wójcikowska & Gaj 2016).

Two major interconnected factors influence the embryogenic potential of explants. The first is the developmental stage of the explant when SE induction takes place. The historic notion holds that temporally younger explants respond better to induction treatments due to their recent loss of developmental potency, but more recent research suggests how that could be irrelevant and that the developmental context of a cell or tissue in combination with the culturing environment plays the key role (Horstman et al. 2017). Genotype of explants plays a significant role too, as witnessed by a study where 350 natural accessions of *A. thaliana* were induced for SE and the efficiency was in the range of 0-92% depending on the genotype. The reasons for this are not completely understood (Wójcikowska & Gaj 2016).

Spontaneous SE is very rare if genetic engineering is not involved, therefore many of the protocols rely on phytohormones for its induction. Of the 17 reviewed protocols, 94% of them used auxin as the sole growth hormone or in conjunction with cytokine, with 65% using solely auxin and 24% also using cytokine (Wójcikowska & Gaj 2016). Phytohormones are usually synthetic chemical substances mimicking the effect of hormones naturally present in plants with better efficiency due to their better chemical stability. 2,4-dichlorophenoxyacetic acid (2,4-D) is the most frequently utilized auxin and N<sup>6</sup>-furfuryladenine or 6-furfurylamino purine (kinetin) is the most frequently utilized cytokinin.

2,4-D is the predominantly used phytohormone for inducing SE *in vitro*. During SE induction, it induces explant cells dedifferentiation and proliferation of embryogenic tissues and sEMB formation. The explanation of its potent effect could lie in its synthetic nature which

excludes it from the metabolic pathways of natural auxin homeostasis. Although the mechanism of this resistance is not known, data suggests that 2,4-D is not subject to dampening of activity through conjugation as is Indole acetic acid (IAA) or other naturally occurring auxins (Enders & Strader 2015). 2,4-D treatment also causes a rise of endogenous auxin in the explant which in turn jump starts developmental reprogramming of cells (Elhiti et al. 2010; Liao et al. 2015). The question persists whether 2,4-D activates the gene regulatory networks specific to SE or does it contribute to endogenous auxin accumulation which then triggers them instead. Although data is not univocal, studies of content of various phytohormones including auxin, have found significant differences in their levels when comparing embryonically competent and incompetent tissues (reviewed by Gaj 2004), further suggesting its importance for *in vitro* embryogenesis promotion.

Cytokinins on the other hand, are utilized in subsequent stages, often in absence of auxin, to incite cell re-differentiation and division. Kinetin was one of the first phytohormones of this class to be isolated (Miller et al. 1955) and remains utilized to this day. Cytokinins have a key role in shoot apical meristem development, in addition to the ability to turn a root lateral primordium into a SAM, they affect flower development and female gametophyte maturation and also play many roles in the root tissues such as maintaining bilateral symmetry, inducing vascular tissue development, determination the meristem size and formation and so on (Wybouw 2018). As for kinetin, Barciszewski et al. (1999) points to how its biological role in *in vitro* manipulations is to induce global transcription, promote cell cycle progression, stimulate intracellular calcium flux while promoting anti-stress effects and relegating anti-ageing properties. It is apparent from these observations that kinetin functions on transcriptional, translational, post-translational and metabolic levels, affecting signal transduction and acting as an anti-oxidant.

Stress has also been identified as a major factor affecting SE. Removal of explants from their physiological surrounding results in production of reactive oxygen species (ROS) that have been found to positively impact SE induction *in vitro* (Elhiti & Stasola 2022). This can be initiated in many ways, such as through osmotic pressure, application chlorides of heavy metals, through pH, by low or high incubation temperature, starvation or mechanical wounding of explants or even tampering auxin levels (Gaj 2004). The suggested explanation of how variable physiological stressors induce embryogenesis is through coalescence of their effects on endogenous auxin levels in cells (Feher 2015). Moreover, Feher states that through the alteration of the physiological hormone levels in cells, they become free of their differentiation

constraints and adapt to their new environment both metabolically and genetically, which results in SE. The elucidation of genomic and especially epigenomic aspects of stress-induced changes of embryogenetic potential and the phytohormone-induced mechanism governing the change will significantly contribute to our understanding of SE.

#### 1.1.4 Somatic embryogenesis in monocotyledons

While SE is studied as a fundamental process in dicotyledonous systems, it is predominantly an important biotechnological tool in monocotyledons. SE is harnessed for regeneration purposes after genetic transformations of monocots and thus, in most commercial systems its importance lies in establishing satisfactory efficacy rates through induction protocol optimization. SE is the preferred system of regeneration because the plants recovered in this manner are not as prone to chimerism brought upon from somaclonal variation occurring in other methods, such as *in vitro* organogenesis. In this chapter I will focus on commonalities in SE induction of the three globally prevalent cereal crops: wheat (*Triticum aestivum* L.), maize (*Zea Mays* L.) and rice (*Oryza sativa* L.). These three cereals, along with many others belonging to the monocot clade exhibit high variability in response to induction treatments. The reasons behind this recalcitrance are poorly understood and are highly dependent upon genetic backgrounds of utilized cultivars.

A traditional SE induction protocols consists of a three to four week-long culturing period of either immature embryos or mature seed explants on media containing 2,4-D in the dark. What follows is a regeneration period on auxin-free media with or without cytokinins and under light conditions (Garrocho-Villegas et al. 2012; She et al. 2012; Verma et al. 2012).

#### 1.1.5 Applications of somatic embryogenesis

Applications of SE are numerous and are relevant both in the academic and the commercial sector. From a commercial point of view, SE's importance is in the ability to efficiently genetically engineer species of interest and to utilize it for scale-up propagation. Protocols for genetic transformation and propagation are developed and utilized for a wide variety of model plants (*Arabidopsis*, *Nicotiana*, *Daucus*), crops (corn, wheat, rice, soybean, sugarcane), perennials (*Pinus*, *Vitis*, *Citrus*, *Coffea*) and pharmacologically attractive plants such as opium poppy (Ochoa-Alejo 2016)



Wehbi (2020) recognizes three major applications of SE. The first is the potential for clonal propagation, the ability to massively and rapidly produce high-quality cultivars from a limited amount of plant material. This is especially impactful because it can be performed year-round in a controlled environment and on genetically preferable plants. The second important application of SE is its use for genetic engineering, the possibility to employ it in creating plants with new and improved characteristics. Better nutritional value or increased tolerance to disease and other biotic and abiotic stresses are much welcome characteristics considering the current global environmental trends. The third major use of SE is its usefulness in obtaining zygotic material which is hard to acquire in larger quantities.

Wehbi (2020) also points out to some major setbacks researchers faces when wanting to utilize SE. One of them is the need to optimize induction media for each species, illustrating how *in vitro* tissue culturing still suffers from trial-and-error methodology. This problem could be alleviated one day through use of SE as a technical tool. The second hardship is the dependency of SE on the genotype of the material used. While many early opinions on regeneration of plant material during *in vitro* cultivation have been challenged and disproven, the problem of recalcitrance to *in vitro* culturing still exists for many species, especially monocots. The final bottleneck of SE utilization is the loss of regenerative ability of tissues kept in culture long-term. This bars exponential multiplication of callus tissue used to produce sEMBs due to unwanted somaclonal variation and lack of proper responsiveness to SE induction. Better methods of cultivation guided by knowledge gathered on genetic effect of culturing and recalcitrance could nullify these bottlenecks.

## 1.2. Monocotyledonous model species *Brachypodium distachyon*

### 1.2.1 General introduction

Since the 1990's, *Arabidopsis thaliana* has become the main model of today's plant science. It has been used to study the mechanisms of plant development, cell biology and genetics, physiology, ecology and evolution. Despite its usefulness as a general model and the plethora of available resources developed throughout the years, it is not always ideal when many of the monocot-specific processes are to be studied. Among the monocotyledonous species, grasses (*Poaceae*) are of a special interest considering that global key crops such as wheat, maize and rice belong to this group. These individual species were proposed in the past as models per se, but their large stature, growth requirements and complex genomes make them demanding models (Betekhtin et al. 2020). Therefore, a more suitable grass model species has been first proposed in 2001 (Draper et al. 2001) and has since come to the forefront of research on grasses. This species is *Brachypodium distachyon* (L.) P.Beauv.

*Brachypodium distachyon* has all the necessary attributes of a model system. It is a self-pollinating, annual temperate grass of small stature, with a short generation time of 8-12 weeks. Growth conditions it requires are fairly simple and the species is easily grown in a controlled environment (Brkljacic et al. 2018). **Figure 1.** represents a schematic overview of a typical protocol of *B. distachyon* transformation and regeneration with indications of main steps and time spans of different phases of the cycle.

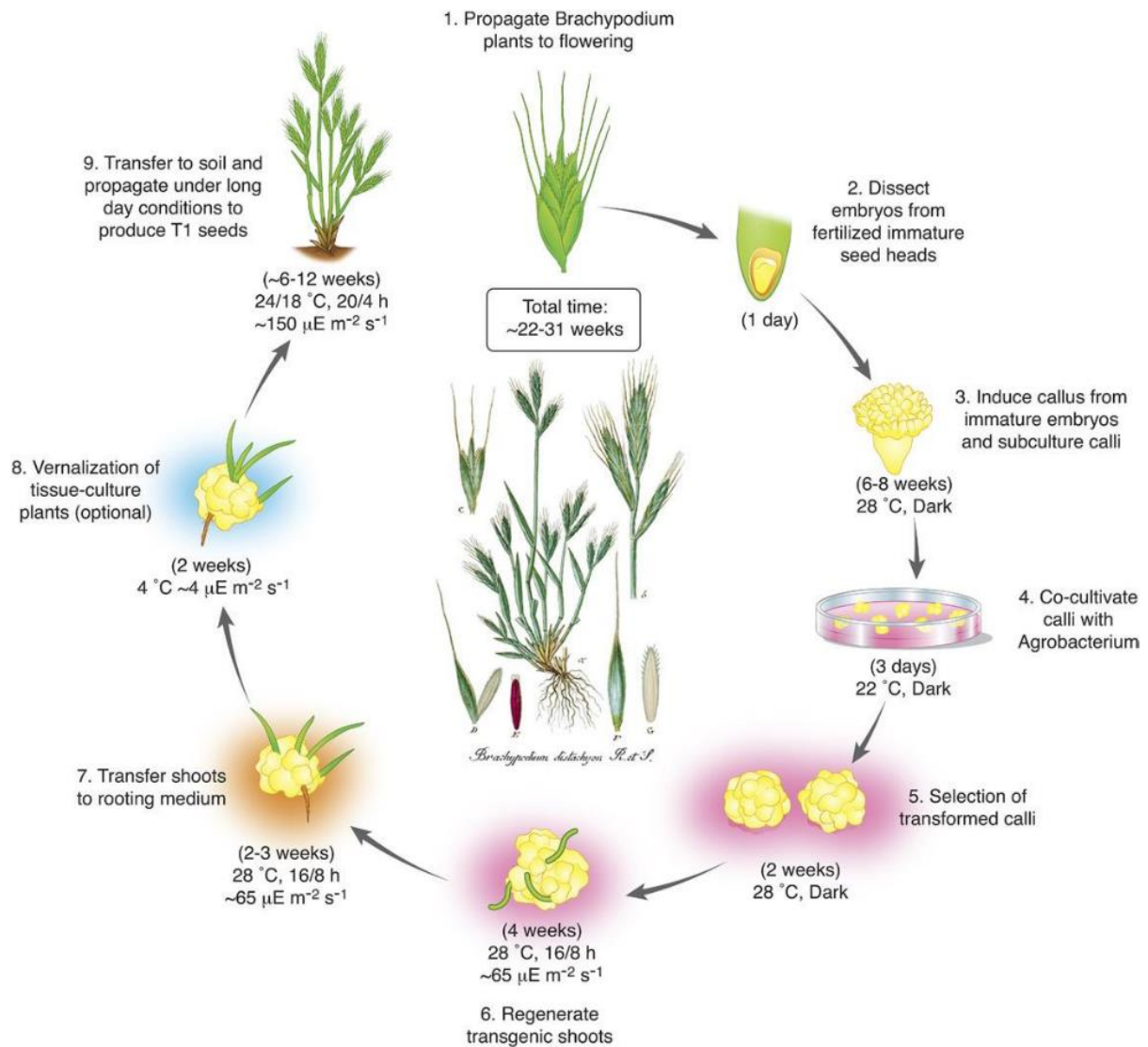


**Figure 1.** Overview of the *Brachypodium distachyon* transformation pipeline. Adapted from Scholthof et al. (2018).

It belongs to the *Pooideae* subfamily of the family *Poaceae*, together with other small grains (important *Triticaceae*, such as wheat, oat and rye) and temperate forage grasses. *B. distachyon* has a small, diploid genome of around 72 Mb (The International Brachypodium Initiative 2010) that is characteristically simple, with genes uniformly distributed between short intergenic distances (Gottlieb et al. 2013). Fully annotated reference genome sequences of the two widely used accessions, Bd21 and Bd21-3, are publicly available through Phytozome (Joint Genome Institute n.d.). Although the genomic complexity of *Triticaceae* presents an obstacle in their research due to its size, polyploidy, high frequency of repeated sequences and transposable elements, it came to light that *B. distachyon* exhibits high genomic synteny to

these species, containing the most conserved loci of other monocots model genomes (Mayer et al. 2011).

Many functional genetics tools are available too, starting with established dataset and sample libraries. These include collections of *B. distachyon* accessions, T-DNA and EMS mutants along with BAC, EST, TILLING and Y2H libraries (Scholthof et al. 2018). Methodological tools for genetic transformation of *B. distachyon* are also well established. The most prominent ones being *Agrobacterium tumefaciens*- and Biolistic-based methods, either through mature or immature embryos (reviewed by Scholthof et al. 2018).

*B. distachyon* as a model system is being used for study of various plant biology topics: grass functional genetics and evolution, the cell wall, flowering, seed development, vernalization and cold acclimation, perenniality and polyploidy, biotic and abiotic stress, root biology, nitrogen use efficiency and plant-pathogen interactions (Girin et al. 2014; Scholthof et al. 2018).

### 1.2.2 Somatic embryogenesis in *Brachypodium distachyon*

As a representative model system in grasses, *Brachypodium distachyon* is usually regenerated through SE following transformation. The core method for induction of SE in *B. distachyon* starts with harvest of immature seeds, approximately 15 days after flowers open (or approximately eight to twelve weeks after seeds were sown) and isolation of embryos 0.3-0.7 mm in size, white in color and with a translucent scutellum edge.

The immature zygotic embryo consists of an embryonic shoot surrounded by the coleoptile and an embryonic root surrounded by the coleorhiza, forming protective sheaths around the growing organs (**Figure 2.**). The embryo proper lies on a triploid endosperm and is connected to the scutellum through parenchymal and vascular tissues. In tissue culture the embryo proper grows similarly to its intact counterparts from the mother plant (Wehbi et al. 2022). However, the embryo proper is irrelevant to SE because the embryogenic tissues arise from the scutellum of the immature zygotic embryo. These embryos are then incubated on the callus-induction medium (CIM) in the dark for three to four weeks. The most important ingredient of CIM is the 2,4-D, with the optimal concentration of approximately 2.5 mg l<sup>-1</sup> (Betekhtin et al. 2020). During the end of this period, two types of calli arise. The one of interest is of yellow color, appearing more compact than the pale white, loosely connected mass it rests

on. This mass represents the other type of callus, one with weak embryogenic potential. The compact, embryogenic callus is usually further divided and subcultured for additional two weeks after which it is used for transformation (Vogel 2007). Regeneration is performed on auxin free-media (Bragg et al. 2014) or auxin free-media containing cytokinin (Oliveira et al. 2017; Wehbi et al. 2022), commonly termed shoot-induction medium (SIM) and it takes three to four weeks before appearance of plantlets. Wehbi et al. (2022) present a notable breakthrough in their publication, having discovered that sEMBs rapidly form after a six day-long induction protocol they designed. With their novel protocol that shortens the week-long callus-inducing phase to a three day-long time period on CIM, they demonstrated that up to 15 individual viable sEMBs can be formed from a single zygotic explant after further three days on SIM. This markedly shortens the overall cycle of regeneration for two to three weeks.

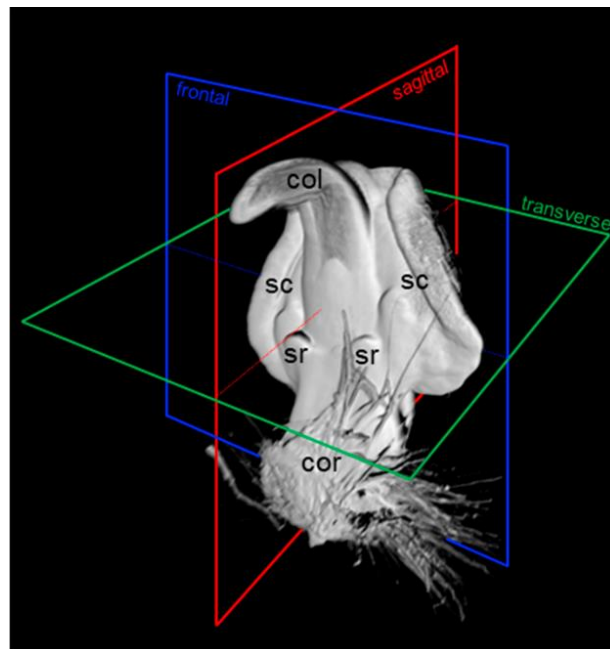


**Figure 2.** 3D reconstruction of the *Brachypodium distachyon* zygotic embryo three days after placement on auxin containing medium. *Abbreviations: col -coleoptile; Continued on next page cor - coleorhiza; emr - embryonic root; ems - embryonic shoot; sc - scutellum; sr - seminal root.* Adapted from Wehbi et al. (2022).

The cellular and histological changes occurring during SE are described using PAS/NBB staining to highlight the cellular content of tissues in question. the periodic acid Schiff (PAS) reagent, which colors polysaccharides in pink was used along with Naphtol blue black (NBB) reagent that marks proteins blue and nuclei dark blue. The combined use of these

stains revealed cell boundaries, starch granules, xylem thickening, and division occurrence. The histological structure of a zygotic embryo three days after placement on auxin containing medium with main tissues indicated by color is illustrated in **Figure 3**.

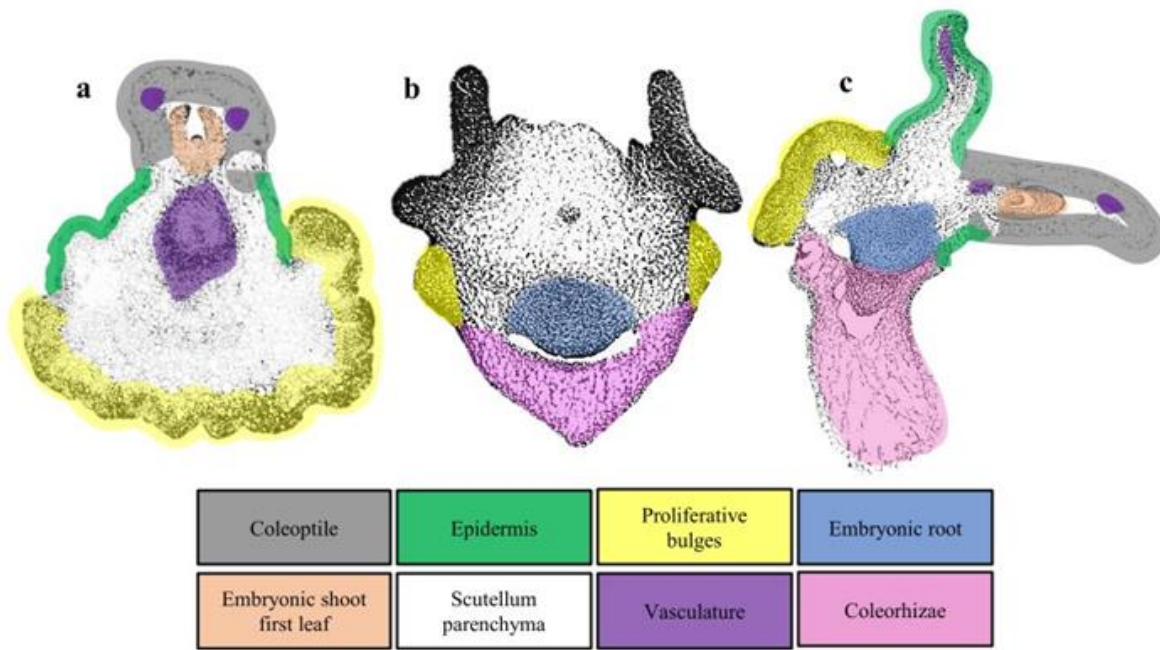


**Figure 3.** Illustration of histological tissues comprising the zygotic embryo undergoing somatic embryogenesis after three days on auxin. (a) Cross-section of a zEMB through the transverse plane (b) Cross-section of a zEMB through the transverse plane. (c) Cross-section of a zEMB through the sagittal plane. Adapted from Wehbi (2020).

Oliveira et al. (2017) described these events occurring during 28 days of SE induction on regeneration media containing kinetin after embryogenic calli were cultivated for three to four weeks using auxin-containing media. They report that before the start of induction on regeneration media, the scutellum tissue is comprised of a single protodermal layer with densely-packed cytoplasm and a compact ground meristem comprised of large parenchymal cells with dense cellular content. After three days of culture, intense periclinal division are detected in both the protodermal and subprotodermal layers with the edge cells being packed densely and the parenchymal ones expanding and becoming vacuolated. In some areas they report callus-like structures forming. In the continuing six to eight days the development of proembryonic zones from the embryogenic callus continues with embryo-like structures

forming around the 21<sup>st</sup> day. These structures exhibit a well-defined protoderm, shoot and root meristems and a closed vascular system, therefore they were identified as sEMBs. At the 28<sup>th</sup> day of culture these newly developed sEMBs were separated from the tissue they arose from. Histological tests performed revealed starch granules in the zygotic scutellum up to the fourth day of induction and again on the 21<sup>st</sup> day, being scattered in the embryogenic tissues. No protein content was detected in cells except for the structural one up to the 21<sup>st</sup> day of incubation and during the whole period, no lipid reserves were detected. Wehbi et al. (2022) confirmed the changes occurring during the callus cultivation phase, additionally remarking that prolonged auxin exposure results only in proliferation of the cellular populations arising from the scutellum already during the first days of incubation on auxin media.

Modifying this classic protocol by shortening the period during which the explants are incubated on auxin, Wehbi et al. (2022) detect some notable events occurring. They were led to experiment with such a short period due to observing how already on the third day of incubation on auxin, the cell displays similar patterns of PAS/NBB coloration as the zygotic embryonic cells. With first division again detected during the second day of incubation and formations of protruding cellular masses on the scutellum on the third day, after a transfer to kinetin-containing regeneration medium, sEMBs are already visible (**Figure 3.**). Between 10-15 of them were identifiable, partially detached and in various stages of early development, containing a clearly established bipolar axis as well as epidermal and vascular tissues. Continuing the incubation on kinetin brought about full development of sEMBs on the sixth day and their complete separation on the ninth. Already on the sixth day they completely resembled the zygotic embryos that they arose from and on the ninth day they could be safely separated and regrown to true-to-type plants. The feature marking dividing cells, proliferative bulges forming on the scutellum and later on proembryogenic masses, was their dark-blue coloration, small size compared to the non-reacting parenchymal cells and lack of starch granules. Such visual cues were present in the zygotic embryonic tissues too, hinting at their shared developmental properties.



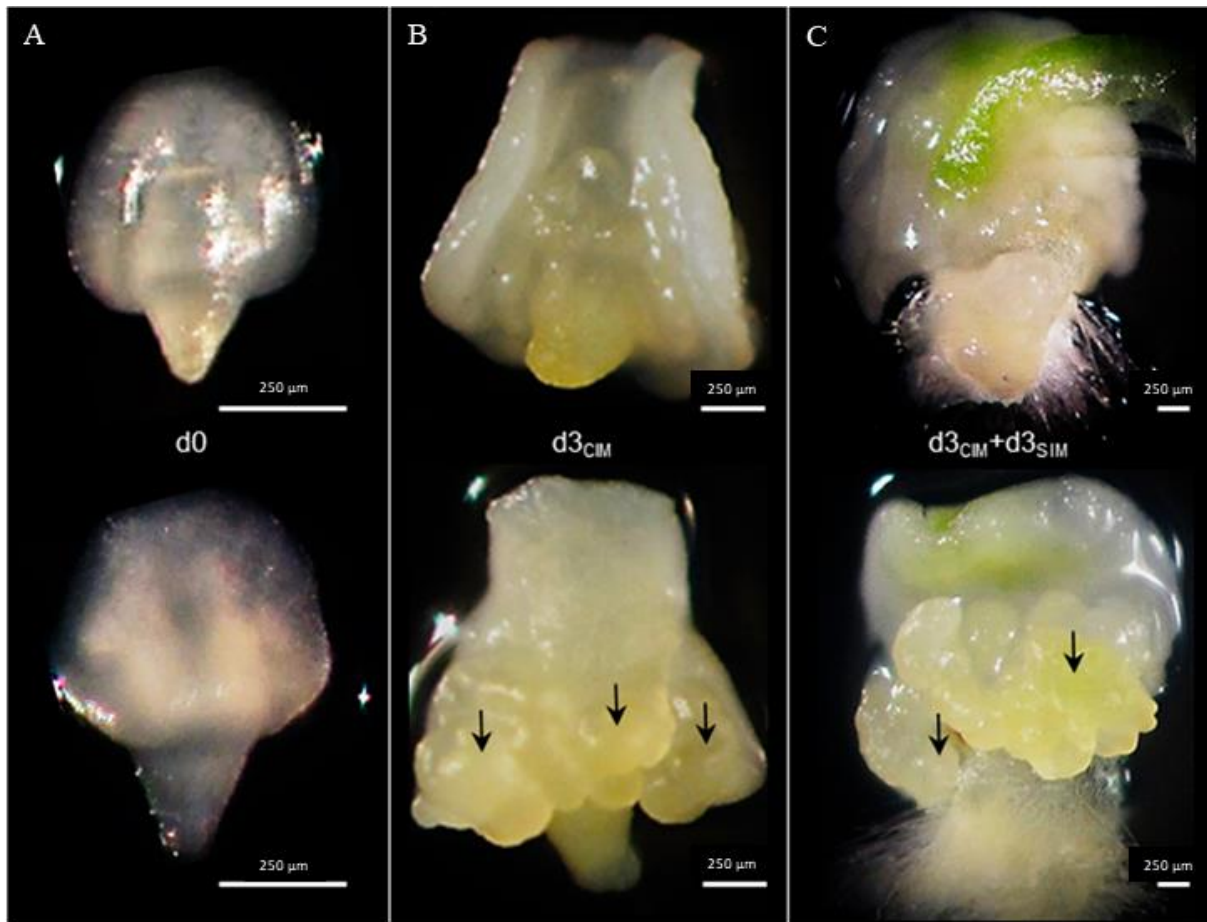


**Figure 4.** Changes occurring in the average *Brachypodium distachyon* explants undergoing somatic embryogenesis. Each panel exhibits the occurrence of changes in the embryo proper (upper image) and the scutellum (lower image). **(A)** The explant before incubation, denoted with d0. **(B)** Explant after three days on auxin-containing medium, CIM (callus-induction medium), denoted with d3<sub>CIM</sub>. Arrows mark emerging proliferative bulges **(C)** Explant after three days on CIM followed by additional three days on kinetin-containing medium, SIM (shoot-inducing medium), denoted by d3<sub>CIM</sub>+d3<sub>SIM</sub>. Arrows mark proembryogenic masses. Adapted from Wehbi et al. (2022).



## 1.3 Effects and control of auxin in plant development

### 1.3.1 Physiological role of auxin

Auxin is the growth hormone of immense importance in plant development, playing a role in local patterning of tissues during embryogenesis and being crucial post-embryonically for continuous iterative production of tissues from both the shoot and root meristem (Leyser 2010). Naturally occurring as indole-3-butyric acid (IBA) and phenylacetic acid (PAA), it is predominantly present as indole-3-acetic acid (IAA). Auxin endogenous levels depend on plant tissue type and its age (seeds usually hold abundant, while developed tissues have significantly lower amounts). Although most tissues have the capability to produce auxin, it is usually produced by the shoot apical meristem, developing fruits, seeds and young leaves in normal growing conditions. Its high presence in the root tip is a product of active transport through the vascular system towards it (Bhatla 2018).

Auxin is biosynthesized from tryptophan which is in turn, produced in the chloroplast. However, the IAA hailing from it can be found mostly in the cytoplasm. IAA is produced primarily through the tryptophan-dependent pathway, with a tryptophan-independent pathway discovered as well. Four tryptophan-dependent pathways exist, which differ in intermediary compounds created. The one prevalent in members of Brassicaceae, Poaceae, and Musaceae is the indole-3-acetonitrile (IAN) pathway: tryptophan is converted to IAA in the presence of nitrilase enzyme with indole-3-acetaldoxime and indole-3-acetonitrile being the intermediates. The tryptophan-independent pathway was discovered in maize loss-of-function mutants for tryptophan synthase. In vitro cultures of this mutant need tryptophan to survive and cannot convert it to IAA but still contain it in high levels. It is hypothesized that the IAA present there originates from indole or indole-3-glycerol phosphate (Bhatla 2018).

To control auxin levels and keep them optimal, so as not to activate a stress response, auxin production is regulated on a biosynthetic level and through degradation. Degradation occurs through conjugation of auxin with glucose, alanine, and leucine, a reversible process that enables sequestration of such conjugates to the vacuole. On the other hand, the oxidative catabolism of IAA is an irreversible process for permanent removal of intracellular auxin not required by the cells. It occurs through chemical modification of indole nucleus or the side chain of IAA, resulting in loss of auxin activity (Bhatla 2018).

Of the many general physiological roles of auxin, the acid growth hypothesis of cell expansion is perhaps the best known one. Occurring due to auxin-stimulated lowering of

apoplastic pH by way of activating membrane-localized H<sup>+</sup>-ATPases, turgor-induced cell expansion is stimulated along with subsequent cell wall synthesis by expansins, whose activity raises with the lowering pH. Auxin is also involved in the mechanisms of apical dominance control, regulated by limiting sugar availability to the axillary buds in intact plants, vascular differentiation where it acts as a vascular inducing signal and “channels” newly differentiated vascular strands and in formation of lateral and adventitious roots through creation of local auxin gradients (Bhatla 2018).

### 1.3.2 Molecular recognition of auxin

Cells perceive auxin through the transcriptional response it causes. The heart of the perception system is the core auxin response module. Its key components are the TRANSPORT INHIBITOR RESISTANT1/AUXIN SIGNALING F-BOX (TIR1/AFB F-box) proteins, the auxin/indole-3-acetic acid (AUX/IAA) transcriptional corepressors and the transcription factors auxin response factors (ARFs) (Li 2017).

F-box-containing (TIR1/AFB) proteins are comprised of the TIR1 and five AFB proteins. These complexes function as auxin receptors by containing an auxin binding pocket which facilitates auxin interactions and also AUX/IAA recruitment. The transcriptional corepressors AUX/IAA interact with the TIR1/AFB complex to form the sensory module for auxin detection. This interaction is facilitated through a degron region and once auxin binds to TIR1/AFB, it becomes a substrate-recognition subunit of the SUPPRESSOR OF KINETOCHORE PROTEIN 1 CULLIN1/F-Box (SKP1/SCF) E3 ubiquitin ligase complex that will execute polyubiquitination that leads to degradation of AUX/IAA protein family. Its removal allows the ARFs to activate or repress early auxin-responsive gene transcription. The role of auxin is compared to glue by Mao et al. (2018) as its presence triggers the formation of protein-protein interactions that lead to transcriptional response through repressor degradation (Li 2017).

There are several factors explaining the variety of responses auxin is known to induce through a system of only three core components. On the part of TIR1/AFB proteins, the members of this family are expressed in certain plant tissues throughout the life cycle with their expression levels varying. In addition, it has been shown that the basis of the wide auxin response potential is due to varying affinity to auxin and various AUX/IAAs. The end result of this is that similar auxin concentration in different cells, and/or different auxin concentrations

in the same cell, might lead to specific developmental responses, depending on the specific members forming the sensory module. The AUX/IAA family of proteins has its role in the diversity of responses as well. Their stability is modulated through the affinity of the SKP1/SCF E3 ubiquitin ligase complex or, to be more precise, through the lysine-arginine amino acid motif that promotes their interaction. AUX/IAAs containing the motif have an increased affinity to SKP1/SCF E3 ubiquitin ligase complex and degrade on lower auxin concentrations, thus modulating the sensitivity of the sensory module. ARFs also play a role in diversity of transcriptional responses through their own diversity. Twenty-three ARF proteins have been identified in *A. thaliana* and loss-of-function analysis experiments demonstrated not only that they control distinct developmental processes but also display some functional redundancy in others (Li 2017).

### 1.3.3 Polar auxin transport

Polar auxin transport (PAT) is the only systemic signal transmission network present in plant tissues, apart from phloem and xylem. PAT network unidirectionally transports auxin from the shoots to the root of the plant. Auxin is the only plant hormone which exhibits polar transport in almost all plants, including bryophytes and ferns (Bhatla 2018). The flow of auxin is determined both by its influx and efflux in cells. A passive aspect of auxin flow is its diffusion in the protonated form across the lipid bilayer of the cellular membrane. This occurs due to the weak acidic nature of endogenous auxins that become protonated in the apoplast due to the pH of 5.5 maintained there. Approximately 25% of IAAH crosses the cell membrane with the concentration gradient and upon entering, becomes deprotonated due to the elevated pH level of the cell (Bhatla 2018).

However, PAT would not be possible without various protein auxin transporters facilitating it. Several of them have been identified, such as AUXIN1/LIKE-AUX1 (AUX/LAX), PIN-FORMED (PIN), ATP-binding cassette (ABC) transporters, nitrate transporter 1.1 (NRT1.1), PIN-Like (PILS) and WALLS ARE THIN 1 (WAT1) transporters (Zhou et al. 2018). The AUX/LAX transporter family is the most prominent group of auxin importers governing its influx. They import auxin into cells through secondary active transport, relying on the proton motive force generated by the pH difference occurring on the two sides of the plasma membrane (Bhatla 2018). On the contrary, two most prominent auxin exporters that determine its efflux belong to two protein families. The first group is the ABC transporter family, members of the multidrug resistance transporter super-family. ABC transporter

subfamilies type B, type D and type G are implicated in endogenous auxin transport. However, they are not expressed in a polar fashion in plasma membranes and thus it is suspected that they do not play a key role in PAT (Gelsier et al. 2017). The second group of proteins are the better studied PINs, usually being in the focus of research due to their polar distribution in the cellular membrane. This difference in distribution across the membrane is exactly what defines the polarity of the auxin transport by directing the auxin through tissues in a coordinated manner (Leyser 2010).

Currently, two hypotheses exist that try to explain the PAT network mechanistically. Both models are based on observations of correlation between auxin and PIN protein presence and thus take the correlation as a primary premise upon which they are constructed. Whether cells contribute to a superimposed auxin pattern solely in its presence, or are they stimulated by a transient pattern to initiate and maintain the pattern autonomously, is not clear. Either way, the dominant models are based on the hypothetical positive feedback loop mechanism between auxin and PIN polarity (von Berkel 2013).

The first hypothesis is the flux-based model, with roots in the Sachs' canalization hypothesis which postulates that cells experiencing flux of a molecule in a certain direction will increase their capacity to transport the molecule in that same direction. Sachs based this theory on observations during vein formation, where auxin transport channels gradually become more and more distinct. Unsurprisingly, this model is regularly used to model vein pattern formation and the PINs that are part of it are expected to point in the direction of the flux. The other hypothesis is the concentration-based model. The core of this model are PIN proteins and their level in the membrane with the hypothesis being that PIN levels increase on the membrane facing the neighboring cell with the highest auxin level. This proposed feedback mechanism was inspired by observations of the shoot apex, where PINs in the epidermal layer orient toward local auxin maxima that develop into organ primordia. These models work well for explaining phyllotactical patterns and the way new maxima form on some distance from old ones with auxin being depleted in their respective neighboring cells (reviewed by von Berkel 2013).

Although these models help to elucidate how auxin flow affects tissue patterning during development, they are still lacking in some aspects. For example, the fountain-like pattern of auxin flow present in the root of *Arabidopsis* cannot be explained by either of them. Therefore, efforts are made to integrate them or develop new ones. For example, the relevance of a model with a more mechanistic approach is being investigated. The model in question is built on the

observation that polarity of PIN proteins coincides stress-related microtubule alignment, the premise being that entry of auxin into the cell causes cell wall stress which in turn influences PIN localization. Other models propose a receptor-influenced distribution of PINs in the sense that the apoplast receptors bind auxin when present and then inhibit local PIN endocytosis (reviewed by von Berkel 2013).

#### 1.3.4 PIN-FORMED auxin transporters

The PIN protein family is a group of auxin efflux carriers that is fueled by the electrochemical gradient across the plasma membrane. To date, PIN genes have been identified in 31 plant species using genome-wide approaches. It is speculated that PIN genes derive from a single ancestor due to higher sequence similarity in between individual genes in higher plants than the similarity of genes with their bacterial homologues. Moreover, they are considered to be unique to land plants originating from streptophyte algae. Their genetic diversity among species is often a product of gene duplications (Zhou et al. 2018).

PINs are divided into two groups, on account of their function and cellular distribution. Nevertheless, they all share a conserved hydrophilic loop with approximately 35 identifiable motifs located between amino- and carboxy-terminal transmembrane domains, likely forming an auxin-translocation pore. Based on the size of the central hydrophilic loop they have been divided into two subgroups, the “long” and “short” PIN proteins. The “short” PIN proteins localize in the endoplasmic reticulum and contribute to cellular auxin homeostasis while the “long” PIN proteins localize at the plasma membrane and facilitate auxin efflux and PAT (Zhou et al. 2018).

PIN genes are regulated through transcription, protein degradation and subcellular trafficking. For example, many *Arabidopsis* “long” PINs are transcriptionally upregulated by auxin which not only generally increases the number and activity of PIN proteins in the plasma membrane but also inhibits PIN internalization. On the other hand, some like PIN2 of *Arabidopsis thaliana* (*AtPIN2*), undergo auxin-mediated trafficking to the vacuole for degradation. An important PIN regulatory mechanism implicated in many developmental processes is the constitutive recycling of PINs. The process is active and clathrin-dependant and can be described as an exchange of the lipid bilayer containing PINs between the plasma membrane and the cellular endosomal compartments. The recruitment of various members of

the PIN family is related to their phosphorylation status which ultimately affects their role in various developmental processes (Křeček et al. 2009).

Individual functions of PIN in the physiological and developmental regard have been only extensively studied in Arabidopsis. Its eight PINs are expressed in different tissues in various developmental stages, have different regulating mechanisms and differing protein structures and cellular localizations. For instance, the prominent PIN1 is involved in the auxin basipetal movement, organ initiation, floral bud formation, leaf shape formation, vein patterning, shoot gravitropic responses and shoot vascular development. PINs *AtPIN3*, *AtPIN4* and *AtPIN7* are on the other hand, connected with the root tissues and are expressed in its meristematic regions, having roles in root patterning and lateral root formation, establishment of the root auxin flux and mediation of the overall root gravitropic response (Zhou et al. 2018). Such a precise assignment of roles has been accomplished for other *AtPINs* as well.

A notable phenomenon of PIN transporters is their redundancy in function. This redundancy does not apply to all the PINs, due to some of them having essential role in key processes of the plant life cycle like the aforementioned *AtPIN1*, essential for development of the aerial parts of the plant and being the sole expressed PIN there during certain developmental stages. However, when there are several PINs present, such as in the mature root tip, where *AtPIN7*, *AtPIN2* *AtPIN3* *AtPIN4* occur, the compensatory functional redundancy is more likely to take effect (Křeček et al. 2009). Such ectopic activity of PINs likely occurs due to the flexible regulation of the promoter regions of PIN genes, with the aim to stabilize auxin gradients and thus contribute to the robustness of the plant adaptive response (Vieten et al. 2005).

### 1.3.5 PIN-FORMED auxin transporters in monocotyledons

Monocots display specific PIN-related features (Forestan et al. 2012). According to phylogenetic studies of PIN sequences, the monocot PIN family is bigger and more divergent, with two or three gene homologues corresponding to one single Arabidopsis PIN gene (reviewed by Forestan et al. 2012). For example, sequence analysis of the twelve PIN genes present in the rice genome revealed that it contains four genes corresponding to the *AtPIN1* gene, three monocot specific PIN genes and no PIN transporters of *Oryza sativa* (*OsPINs*) grouping in the *AtPIN3*, *AtPIN4*, *AtPIN7* cluster. As for the *AtPIN1* homologues, *OsPIN1a* and *OsPIN1b* showed a constitutive expression, *OsPIN1c* is mainly expressed in root and stem while the expression pattern of *OsPIN1d* was not characterized (Wang et al. 2009).

Furthermore, Forestan et al. (2012) reports identification of 12 maize PIN genes, adding on their previous analysis of PIN transporters of *Zea mays* (*ZmPINs*) functions in which they report the expression of the four maize *AtPIN1* homologues. The homologues are *ZmPIN1a* and *ZmPIN1b* which have ubiquitous expression patterns, *ZmPIN1c* which is preferentially expressed in the post-embryonic root and stem and *ZmPIN1d* which shows a high expression specificity, marking the transition from the vegetative to the reproductive development in shoot apical meristems and inflorescence meristems (Forestan et al. 2010). As for the other *ZmPINs*, their expression analysis in major maize tissues pointed to a significant degree of overlap in expression, unlike in *A. thaliana*, where each *AtPIN* is expressed in a specific domain.

The high tissue-specific regulation and expression of individual *ZmPIN* genes during various developmental stages was detected too, as was in rice. This indicates the occurrence of subfunctionalization of monocot PIN in their developmental and physiological roles, in spite of their partial overlap in expression occurrence (Forestan et al. 2012).

### 1.3.6 PIN-FORMED auxin transporters in *B. distachyon*

Likewise, a number of PIN genes has been identified in the model monocot *B. distachyon* (Hillson & Wehbi 2020, unpublished raw data). Among the 11 PIN transporters of *Brachypodium distachyon* (*BdPIN*) genes, the three most studied genes are the *AtPIN1* homologues *BdPIN1a*, *BdPIN1b* and *BdSoPIN1*. *BdSoPIN1* is a member of a clade of PIN proteins absent from *Brassicaceae* and present in most other Angiosperms (O'Connor et al. 2014.) and thus named Sister-of-PIN1 (SoPIN1). By reconstructing the phylogenetic relationship of *Brachypodium* SoPIN1, PIN1a and PIN1b to *Arabidopsis* PIN1 (**Figure 5**), they revealed that the two *BdPIN1* belong to a sister clade of *AtPIN1*.

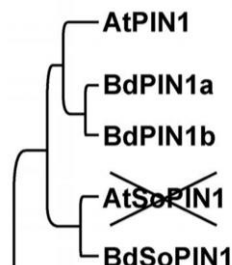


**Figure 5.** Inferred phylogenetic relations among some of the PIN transporters of *A. thaliana* and *B. distachyon*. The crossed out *AtSoPIN1* represents its loss and absence in *A. thaliana*. Adapted from O'Connor et al. (2014).

Studying the role of the particular *BdPINs*, during initiation of the lemma, a leaf-like floral organ in the *B. distachyon* from which seed-bearing spikelets form, lead to conclusions on their respective roles. *SoPIN1* was found to be highly expressed in the epidermis, polarized towards presumed auxin maxima, and forming convergent polarization patterns, suggesting a role in creating the auxin maxima required for organ initiation in the shoot. *BdPIN1a* and *BdPIN1b* were expressed in a contrasting fashion, primarily in the subepidermal tissues following auxin maxima initiation and during the tissue patterning phase. Moreover, they were weakly expressed in the epidermis and oriented away from presumed auxin (O'Connor et al. 2014; O'Connor et al. 2017). Using computational models, the authors also showed how these patterns can emerge assuming a combined effect of *SoPIN1* polarizing up the gradient of auxin concentration and *PIN1* members polarizing with the auxin flux. In other words, *SoPIN1* polarizes in individual cell membranes, “up-the-gradient” and towards the neighboring cell with the highest auxin concentration, while *PIN1a* and *PIN1b* polarize ‘with-the-flux’ accumulating in the membrane experiencing the highest net auxin efflux.

In summary, O'Connor et al. (2014) proposed the following roles for individual *BdPINs* during shoot formation: *SoPIN1* forms convergence points which determine the sites of organ initiation and position of veins while *PIN1b* directs the developing veins to target locations with *PIN1a* transforming broad regions of polar auxin flux into narrow canals. They postulate how the actions of the three *BdPINs* create a singular auxin flow in the shoot, despite their unique distributions and polarization patterns.

Function-based division is proposed for the *SoPIN1* and *PIN1* clades as well, supported by observations such as their conserved presence throughout angiosperms, opposing polarities on a cellular level and differences in protein sequence between the clades. Interestingly, these differences are in the region of the protein containing phosphorylation sites involved in *PIN1* localization in *A. thaliana*, suggesting that different regulation pathways control their cellular localization (O'Connor et al. 2014; O'Connor et al. 2017).

As for functional similarity of *BdPIN1s* and *BdSoPIN* their sister clade *AtPIN1*, O'Connor and al. (2017) point out how the combined expression domains and polarization behaviors of *SoPIN1*, *PIN1a*, and *PIN1b* in *Brachypodium* largely recapitulate those observed for *PIN1* alone in *A. thaliana*. *AtPIN1* converged in neighboring cells around the initiation sites of new organs, suggesting that it concentrates auxin into local maxima causing organ initiation.



It is worth to mention the effect of loss-of-function mutations for these three *BdPINs* on organ initiation in the apical shoot meristem. The SoPIN1 mutants yielded barren inflorescences, without seed-bearing organs while the PIN1 clade mutants had very little effect on inflorescence formation although such plants exhibited a change in internode length (O'Connor et al. 2017). These findings accentuate the importance of SoPIN1 in *B. distachyon*, but at the same time present us with a phenomenon where apparently different species rely differently on their PINs. For example, SoPIN1 clade mutants' in *Medicago truncatula* and tomato (*Solanum lycopersicum*) do exhibit pleiotropic defects in their development but are still able to develop seed-yielding inflorescences (Martinez et al. 2016; Zhou et al. 2011).

### 1.3.7 Experimental methods for tracking auxin

Biosensors and reporters of auxin enable the visualization of auxin dynamics and distribution and therefore allow researchers to analyze how its presence mediates growth and developmental processes. The goal of any analysis is establishing the location of auxin maxima and minima and the concentration gradients in between so the overall auxin flux in the tissues and organs can be deduced. The many available systems allow researchers to visualize it by hijacking some of the cellular mechanisms connected to auxin sensing and response (Jedličková et al. 2022).

Transcriptional reporters are the most popular and widely used due to the simple way they function and can be assessed. The core of these reporters is a promoter of an auxin-responsive gene or an artificially created promoter that drives expression of a reporter gene. The first constructs had the promoters of various genes detected to be induced by auxin cloned upstream of the  $\beta$ -glucuronidase (GUS) or green fluorescent protein (GFP) (Hagen et al. 1991; Pacios-Bras et al. 2003). The discovery that enabled the design of synthetic promoters with better inducibility was the identification of AuxRE sites containing a core TGTCTC motif that confers their inducibility (Boer et al. 2014). An AuxRE motif hailing from soybean Gretchen hagen gene 3 (GH3) with a coupling element tied to the core sequence titled D1-4 was modified by two thymidine substitutions and so, the DR5 (5'-CCTTTTGTCTC-3') promoter core sequence was generated. The frequently used reporter genes coupled to the DR5 promoter construct include GUS or firefly luciferase (LUC) or various iterations of GFP. DR5v2 was developed as well, with the core promoter sequences based on motifs of various ARF interaction sequences which had better affinity towards it. Use of DR5v2 allowed to detect even

more sensitive auxin responses than with the original motif. DR5 and other derived reporters are indirect reporters that monitor the nuclear transcriptional auxin response by activating reporter genes. This group of reporters can therefore be considered auxin output reporters. A downfall of this system is that variations in reporter signal intensity exists and evidence points to divergence in spacing between AuxRE between species as the culprit (Boer et al. 2014). Another aspect of the differing intensities could be the natural physiological variance between species which affects cell wall properties that govern permeability of the phytohormones. All in all, considering how this system was optimized for *Arabidopsis*, modifications could be necessary if results are unsatisfactory in other systems (Jedličková et al. 2022).

The disadvantage of the DR5-based reporters is that its activity reflects the auxin signaling output rather than the phytohormone concentration itself. To address the question of distribution of auxin per se and its concentration in cells, reporters based on the auxin-interacting degradation domain II (DII) have been designed. This kind of constructs serve as auxin input reporters.

The first of such reporters is DII-VENUS (Mir et al. 2017; Yang et al. 2017). It is a genetic construct under a constitutive promotor containing the auxin-interacting domain DII, harboring a 13-amino acid long degron motif necessary for the interactions that lead to degradation and VENUS, a fast maturing variant of the yellow fluorescent protein. The DII-VENUS protein is degraded in the presence of auxin through the same pathway the AUX/IAA repressive co-receptors are after ubiquitination by the SCF ubiquitin ligase complex. In this manner, DII-VENUS signal depends on both the concentration of active auxin and moreover, it is negatively correlated with auxin presence.

The positive side of this kind of reporter is that it is better correlated with phytohormone abundance in the cell than DR5. Also, it shows the areas of auxin minima and thus can be used in conjunction with DR5 analysis. It is also very rapid in its response, taking minutes where it took up to two hours for transcription-based reporters (Brunoud et al. 2012).

Thanks to the dynamism of this system, quantification is possible as well. Liao et al. (2015) developed such a system, naming it R2D2 (Ratiometric version of two DIIs). It was created by cloning the DII-VENUS cassette downstream of the ribosomal protein subunit 5A (RPS5A) promoter, which is active in most dividing cells. Then this combination was placed in-frame and upstream of the sequence encoding nucleus-targeted VENUS with another expression cassette consisting of RPS5A promoter-driven mDII and a gene for nucleus-targeted

tdTomato (a red variant of the GFP). This way, a single transgene contains two fluorescent reporters whose signal intensity can be compared and through depletion of the VENUS reporter, relative auxin quantities can be deduced.

The downside of degron-based reporters concerns their dependence on presence of auxin sensory systems in the cells and this can lead to tissue-dependant specificity and varied responsiveness to auxin. Also, the broad variability of the amino acid sequence in the degron region influences interaction that could lead to lower stability of VENUS or, in other words, higher rate of degradation that does not reflect auxin abundance (Jedličková et al. 2022).

## 2. AIM OF RESEARCH

---

The goal of this research is characterization of SE in the monocot model species *B. distachyon* with a special focus on the early histological events occurring during SE initiation and induction. Distribution of *B. distachyon* PIN-FORMED auxin transporters PIN1a, PIN1b and SoPIN1 during initiation and induction of SE are used as criteria for monitoring auxin flow and localization of auxin-induced changes. Along with this, phenotypic traits of explants of loss-of-function mutants *pin1a*, *pin1b* and *pin1a* × *pin1b* are examined on a histological level to determine whether these PIN transporters play a key role during the onset of SE.

The main hypothesis underlying the research is that the *B. distachyon* PIN-FORMED auxin transporters PIN1a, PIN1b and SoPIN1 jointly shape the auxin flow that is in essence the physiological cue imperative for induction of SE.

## 3. MATERIALS AND METHODS

---

### 3.1 Materials

#### 3.1.1 Plant material

The immature zygotic embryos I used for examination of *in vitro* SE induction originated from previously created lines, all of them originating from the Bd21-3 accession of the model monocot *Brachypodium distachyon* (L.).

I used three fluorescent marker-containing lines derived from the accession Bd21-3 for the purpose of exploring the distribution of selected PIN-FORMED proteins under their native promoters along with the presence of auxin.

The marker lines are:

- (i) line expressing a fluorescent fusion protein PIN-FORMED1a-Citrine under a native promoter of *B. distachyon* PIN1a
- (ii) line expressing two fusion proteins, PIN-FORMED1b-Citrine and SoPIN1-Cerulean under their native promoters along with a DR5-based reporter, a synthetic auxin transcriptional reporter consisting of the DR5 promoter sequence driving the expression of an endoplasmic reticulum-localized monomeric RFP (O'Connor et al. 2014)
- (iii) line containing the DII-VENUS auxin response sensor, consisting of a fusion of a YFP-derived VENUS fluorescent protein coupled to a Aux/IAA interaction domain containing an *Arabidopsis*-derived degron and expressed under a constitutive maize ubiquitin promoter (ZmUbi) (Brunoud et al. 2012)

The creation of the lines (i) and (iii) is described in depth by O'Connor et al. (2014). Line (ii) was created from crosses of transgenic plants published in O'Connor et al. (2014) and has no available publishing record itself. All of them were obtained beforehand thanks to the kindness of Devin O'Connor, PhD.

I utilized three loss-of-function mutant lines, along with a reference wild-type line for histological characterization of somatic embryogenesis defects. All of them are derived from the inbred line Bd21-3 and were created previously by CRISPR/Cas9 mutagenesis (O'Connor et al. 2017). These lines were sourced from the author personally as well.

Two of the three lines exhibit a loss-of-function mutation either for *pin1a* or *pin1b* protein. The third line (*pin1a* x *pin1b*) originates from a cross between the two homozygous lines, having a loss-of-function mutation for both proteins.

### 3.1.2 Greenhouse cultivation substrate

The seeds of the fluorescent tag-carrying lines as well as those of the loss-of-function mutant lines were grown in a mixture of peat moss supplemented with a basic NPK fertilizer (B 400 with Cocopor® - Stender AG). The fertilizing solution contained only essential macro-nutrients. Its composition is further outlined in **Table 1**.

**Table 1.** Composition of fertilizing solution, 200x concentrated.

Macro-elements	Quantity utilized
58% nitric acid, HNO <sub>3</sub> (d=1.367;38.9°Be)	2.6 L
Soluble fertilizer (NPK 15-10-30)	15 kg
dH <sub>2</sub> O	100 L

### 3.1.3 Plant nutrition media

I utilized two types of media for induction of somatic embryogenesis, the main difference being the plant growth hormone they contain. Callus-induction medium (CIM) contains synthetic auxin plant growth hormone 2,4-Dichlorophenoxyacetic acid, 2,4-D (*Sigma-Aldrich*) while the Shoot-induction medium (SIM) contains kinetin (*Duchefa-Biochimie*), a synthetic cytokinin analog. Detailed compositions of the media are outlined in **Table 2**. and **Table 3**. The immature embryos were cultivated in petri dishes with a circumference of 96 mm and containing 25 mL of autoclaved media.

**Table 2.** Composition of Callus-induction medium (CIM), pH 5,7

Ingredients	Quantity
Murashige&Skoog medium powder with vitamins (reference n <sup>o</sup> MO2222, <i>Duchefa Biochimie</i> )	4.4 g
Sucrose ( <i>Duchefa Biochimie</i> )	30 g
PhytigelTM ( <i>Sigma Life Science</i> )	2 g
CuSO <sub>4</sub> (0,6 mg/mL)	1 mL
2,4-D (2,5 mg/mL)	1 mL
dH <sub>2</sub> O	1000 mL

**Table 3.** Composition of Shoot-induction medium (SIM), pH 5,7

Ingredients	Quantity
Murashige&Skoog medium powder with vitamins (reference n <sup>o</sup> MO2222, <i>Duchefa Biochimie</i> )	4.4 g
Maltose ( <i>Duchefa Biochimie</i> )	30 g
PhytigelTM ( <i>Sigma Life Science</i> )	2 g
Kinetine (0,2 mg/mL)	2 mL
dH <sub>2</sub> O	1000 mL

Both media were batch sterilized before being poured into petri dishes under sterile conditions. Media were sterilized using a Horizontal Steam Sterilizer (*PROHS*<sup>®</sup>) and the available Standard Program for Porous Loads.

## 3.2 Methods

### 3.2.1 Greenhouse cultivation of plant material

The seeds of the fluorescent tag-carrying lines and the ones of the loss-of-function mutant lines were grown in a controlled greenhouse environment. The conditions consisted of an 18 hour-long light photoperiod followed by 6 hours of dark. The daily temperature varied between 22 °C to 24 °C and was kept at 20 °C during the dark period. Relative humidity was kept constant at 60%. The plants were watered twice-daily with a volume of 160 mL of fertilizing solution per pot. The fertilizing solution contained only essential macro-nutrients and is described in chapter 2.1.2. The growth conditions are further outlined in **Table 4**.

**Table 4.** Daily climatic conditions used for cultivation of Bd21-3 ascension-derived lines.

	Dawn	Day	Dusk	Night
Start of time period	4:00 AM	5:00 AM	21:00 PM	22:00 PM
Light intensity	210 $\mu\text{mol m}^{-2} \text{s}^{-1}$	280 $\mu\text{mol m}^{-2} \text{s}^{-1}$	210 $\mu\text{mol m}^{-2} \text{s}^{-1}$	0 $\mu\text{mol m}^{-2} \text{s}^{-1}$
Temperature	22°C	24°C	22°C	20°C

### 3.2.2 Harvesting and sterilization of plant material

I hand-harvested spikes of *B. distachyon* lines containing the immature zygotic embryos approximately two months after germination and between 14 to 16 days after emergence of first visible inflorescence on individual plants. The spikes were collected based on physiological cues pointing to their ripeness such as green coloration of the spike, visibility of anthers inside seeds and tactile perception of seed firmness.

I surface sterilized the harvested spikes by incubating them for 30 minutes in a sterilizing solution consisting of one mini Bayrochlor® tablet (*Bayrol*) and 1 mL of Domestos® bleach dissolved in 800 ml of tap water. The sterilizing solution containing the spikes was agitated with a magnetic stirrer. Following this treatment, I rinsed the spikes three times with sterile water under a laminar flow hood. Spikes were kept moist afterwards to ease extraction of embryos.

### 3.2.3 Isolation of immature zygotic embryos

I hand-isolated the immature zygotic embryos of all *B. distachyon* lines utilized under sterile conditions. The 0.4 - 0.6 mm embryos were isolated mechanically, using a scalpel and tweezers, by separating the individual seeds from the spikelet before dissecting them and taking the embryo. Owing to the size of the plant material, I used the Nikon SMZ 745 (*Nikon Instruments*) stereo microscope during the process.

### 3.2.4 Somatic embryogenesis induction

Once I isolated and selected appropriate zygotic embryos which were expected to react to SE-inductive conditions *in vitro* most optimally (following the protocol described by Wehbi et al. 2022), I placed them in 96 mm petri dishes containing 25 mL of autoclaved CIM media.



Individual petri dishes were sealed with parafilm and incubated for 72 hours in dark, in a growth chamber with a temperature of 28 °C and relative humidity of 60%.

The explants were afterwards transferred under sterile conditions to SIM for 72 hours of incubation. They were incubated under a 16-hour light photoperiod with light intensity of 60  $\mu\text{mol m}^{-2} \text{s}^{-1}$  and with 8-hour dark, under a constant temperature of 28°C and 60% relative humidity.

This exact procedure was applied to both the fluorescent tag-carrying explants and loss-of-function mutation-carrying explants.

### 3.2.5 Preparation of fluorescent tag-carrying explants for confocal microscopy

During the six combined days of embryo's CIM and subsequent SIM medium incubation, I sampled the fluorescent tag-carrying explants every 24 hours, starting from the moment they were placed in incubation. These periods were chosen due to previously made observations on key temporal windows during which important events of SE occur (Wehbi et al. 2022). A number of explants were taken from a population of incubating explants while the ones not collected were left for future samplings. I dip-incubated the collected ones in a 4% paraformaldehyde solution created by diluting a 36% paraformaldehyde stock solution (*Sigma-Aldrich*) in 1x PBS buffer (*euobio Abcys*) with extra added 0.1% Triton™ X-100 detergent (*Sigma-Aldrich*) to fix the samples. The incubation period lasted for 45 minutes and the samples were agitated on a mechanical shaker.

Afterwards, I rinsed the fixed explants twice in the 1x PBS buffer with added 0.1% Triton™ X-100 detergent and placed them in 3 mL of ClearSee solution for a period of at least 5 and up to 8 days, depending on the size of the explant. ClearSee is a preparation that renders fixed explants transparent, allowing deeper penetration into tissue layers during imaging of fluorescent signals (Kurihara et al. 2014). It is an aqueous solution consisting of following reagents in powder form: Xylitol (*Sigma-Aldrich*) at 10%, Sodium deoxycholate (*Sigma-Aldrich*) at 15% and Urea (*euobio Abcys*) at 25% of final mass concentration.

I also added Fluorescent brightener 28 (*MP Biomedicals*) better known as Calcofluor white, a cell-wall staining solution with fluorescent properties, to explants originating from lines (i) and (iii) at 0.1% final mass concentration. This was done to accentuate cell-walls during

imaging of objects with Calcofluor white being bound to cellulose. Samples obtained from the line (ii) were not treated such due to Calcofluor white's emission wavelength overlapping with the one of RFP from the DR5 auxin transcription response marker.

Samples were mounted just before viewing on microscopy slides containing a concave cavity in 1% low gelling temperature Agarose (*SIGMA Life Science*).

### 3.2.6 Microtome section preparation for staining of loss-of-function mutants

I sampled the loss-of-function mutant explants *pin1a*, *pin1b* and *pin1a* × *pin1b* along with a wild-type Bd21-3 explant line after 72 hours of incubation on CIM and after additional 72 hours of incubation on SIM medium. A number of explants were taken from a population of incubating explants while the ones not collected were left for future samplings. These periods were also chosen based on observations previously made on key temporal windows of SE (Wehbi et al. 2022).

I immersed the selected explants in a precipitating fixator RCL2<sup>®</sup> (*Excilone*), a formalin-free, non-toxic, ready-to-use commercial solution. I placed them in 3 mL of the solution and kept them under vacuum for 30 minutes, removing the holding containers from the vacuum afterwards and leaving the samples to incubate overnight.

Following the overnight incubation, I gradually dehydrated the explants with a series of ethanol baths of growing concentrations. The gradient started with 70% ethanol bath, continued with an 80% and 96% ethanol baths and finished with two separate immersions in absolute ethanol. Incubation period in each ethanol concentration was one hour. The samples were further kept in absolute ethanol on 4°C.

The next step of the treatment was substituting the ethanol with Histo-Clear<sup>®</sup> II (*Electron Microscopy Science*), a non-toxic clearing agent. I incubated the explants in baths with gradually higher parts of Histo-Clear<sup>®</sup> II, starting with 2:1 absolute ethanol: Histo-Clear<sup>®</sup> II bath, continuing with a 1:1 absolute ethanol: Histo-Clear<sup>®</sup> II bath and finishing with a 1:2 absolute ethanol: Histo-Clear<sup>®</sup> II bath. Afterwards, I incubated the explants in pure Histo-Clear<sup>®</sup> for 90 minutes all the while changing the Histo-Clear<sup>®</sup> II incubation solution every 30 minutes.

The final step before embedding was substituting the Histo-Clear<sup>®</sup> II with paraffin (Surgipath Paraplast Plus, *Leica*). I started this procedure by transferring samples into dedicated

porous containers and incubating them in a 1:1 Histo-Clear® II paraffin solution for an hour at 60 °C before continuing with a 36 hour-long incubation in pure paraffin. Finally, I transferred the explants to molds destined for cutting and, after an overnight hardening on room temperature, stored them on 4 °C.

I cut the paraffin blocks containing embedded explants using a Leica RM2165 microtome to sections of 8 to 12 µm thickness, determined by the quality of cuts being produced. I placed the created cuts on *in situ* hybridization slides (Xtra Adhesive Precleaned microslides, *Leica*) and left them to hybridize overnight at 37 °C.

### 3.2.7 Staining of loss-of-function mutant tissue sections

I stained the *in situ* hybridization (ISH) slides containing the tissue sections of the loss-of-function mutant explants with Periodic Acid Schiff (PAS) and Naphtol Blue Black (NBB) dyes. All steps were done at room temperature.

First, I immersed the slides in two consecutive baths of pure Histo-Clear® II (*Electron Microscopy Science*) for 10 and 15 minutes respectively and then followed through with two consecutive immersions in absolute ethanol lasting a minute each. Afterwards, I washed the tissue sections on slides with 1% periodic acid (*MM France*) for 5 minutes and quickly rinsed them under distilled water before immersing them in the Schiff reagent (*VWR chemicals*) for 10 minutes in the dark. Then, I transferred the slides to a Sulphur bath solution (sodium metabisulfite (*Sigma-Aldrich*), 5 ml; hydrochloric acid N (*VWR chemicals*), 5 ml; distilled water, 90 ml) for 5 minutes and washed them with distilled water until the water stayed colorless after slide removal. I applied Naphtol Blue Black staining (*Sigma-Aldrich*) 1 g; acetic acid 7 ml; distilled water QSP 100 ml) by heating the staining solution to 60°C and incubating slides carrying the sections in the heated colorant for 5 minutes. Afterwards, I quickly washed them in distilled water and treated them with 7% acetic acid diluted with distilled water before leaving them to dry overnight. Finally, I covered all the slides with cover slips after adding a drop of CoverSafe mounting medium (*Quimigen*).

### 3.2.8 Confocal microscopy

I imaged mounted samples of explants undergoing somatic embryogenesis originating from fluorescent tag-carrying lines on the Leica confocal microscope system, model TCS SP8

SMD. I made the observation of samples as well as image acquisition using the Leica Application Suite X (LasX) software, version 3.5.7.23225 (*Leica microsystems*).

Due to the nature of the preparation protocol for microscopy, I was not able to observe the same explants in a temporal developmental sequence. Instead, I analyzed multiple explants hailing from the same mother plant at similar developmental stages, captured at the 24-hour sampling time periods. In other words, the results represent a theoretical developmental sequence of events reconstructed in the basis of analysis of many objects which all underwent the same process of *in vitro* SE induction.

Explants were observed through the 20x magnification dry objective with 0.75 numerical aperture (HC PL APO 20x/0.75 CS2 *Leica microsystems*) as well as on the 40x magnification plan apochromatic oil immersion objective (HC PL APO 40x/1.30 Oil CS2, *Leica Microsystems*) with 1.30 numerical aperture. The excitation and emission wavelengths for fluorophores observed are as follows: Citrine was excited at 405 nm and the emitted signal caught was in the range of 425 to 475 nm, Cerulean was excited at 422 and observed in the range of 470 to 520, VENUS was excited at 512 and the emission was observed at 520 to 560 nm, RFP was excited at 561 and observed on 588 to 633 nm. Finally, Calcofluor white was excited at 405 nm and observed at 425 to 475 nm. The wavelengths were based on work performed by O'Connor et al. (2014) and O'Connor et al. (2017) and ultimately adjusted for optimal results on the available confocal system.

Detection gain and laser power were varied and optimized for best resolution since no quantitative measurements were taken. Fluorescent channels were processed with a median filter to reduce noise and are presented as single z-plane sections or as maximum intensity projection images which reveal an overlay images of all planes. I adjusted brightness and contrast for optimal visibility after fluorescence channels were pseudo-colored with look-up tables. During image collection, focus was given to capturing the events occurring in the scutellum of *B. distachyon* as previous finding indicated it as the tissue of greatest interest for SE occurrence (Wehbi et al. 2022).

### 3.2.9 Bright-field microscopy

The explants analyzed and presented in this paper here come from various zygotic embryos originating from the same mother plants and have all gone through the same process

of *in vitro* SE induction. The most informative stained tissue section cuts are shown and conclusions made are based on theoretical sequences of developmental events inferred from observing many objects.

I observed and photographed these PAS/NBB stained and mounted sections of the loss-of-function mutant lines as well as the reference wild-type line with a Zeiss microscope, model AxioZoom V16 fitted with the Axiocam 512 color camera. For this purpose, I used the Zen 2.6 (blue edition) software, version 2.6.76.00000 (*Carl Zeiss Microscopy GmbH*) and various magnifications. During image collection, focus was given to capturing the events occurring in the scutellum of *B. distachyon* as well, indicated by previous findings (Wehbi et al. 2022).

## 4. RESULTS

---

### 4.1. Distribution of PIN1a during somatic embryogenesis

Tracking of PIN1a-Citrine during the consecutive days of SE induction revealed how it is expressed continuously throughout SE induction in the *B. distachyon* system. Before zygotic embryos are placed on the callus-induction medium (D0<sub>CIM</sub>), the PIN1a-Citrine signal appeared to be located on their dorsal side, inside the scutellum (**Supplemental Figure 1. A**). At this point the scutellum consisted of two major cell types, discernible due to their sizes. The smaller epidermal cells arranged in a palisade manner and the subepidermal layers of parenchyma-like cells of larger stature (**Figure 6. A**, marked with a dotted circle). Examining a confocal cross-section of the embryo revealed the presence of the PIN1a-related signal in cellular clusters of parenchymal cells (**Figure 6. A**, marked with yellow arrows). These clusters surrounded closely the strands of vascular tissue (**Figure 6. A**, white arrow marks the main vascular strand of the embryo). The signal present in these cells was not membranous but appeared to be vesicular (data not shown).

Following 24 hours of incubation on CIM (D1<sub>CIM</sub>), signal intensity in the scutellum increased, especially in the lower dorsal area of the embryo, adjacent to the coleorhiza (**Supplemental Figure 1. B**). The intensity levels of the signal in the parenchymal cells appears to have risen compared to observations of D0<sub>CIM</sub>, and the signal is now localized mostly in the plasma membranes (**Figure 6. B**, marked with a white dotted circle). Nevertheless, in certain parenchymal cells the signal was present in the cytoplasm and it also was not present in the epidermal cells (**Figure 6. B**, marked with a yellow dotted circle).

After 48 hours on CIM (D2<sub>CIM</sub>), the signal distribution patterns were notably different. The overall presence of PIN1a-Citrine in the scutellum was limited mostly to the area adjacent to the coleorhiza, where bulging of tissues and appearance of invaginations occurred (**Supplemental Figure 1. C**, marked with a dotted circle). The signal inside these bulging areas was mostly localized to plasma membranes and present either in small, irregularly shaped cells located between parenchymal and epidermal cell types (**Figure 6. C**, marked by a white dotted circle) or in the subepidermal, parenchymal cells (**Figure 6. C**, marked by a yellow dotted circle).

After 72 hours on CIM (D3<sub>CIM</sub>), growth of the proliferative bulges appears to have continued. The bulging progressed to a point where invaginations started to divide these newly present cellular masses (**Supplement Figure 1D**, marked with dotted circles). Inside them, a

novel pattern of PIN1a-Citrine was established. The epidermal side of the bulge, more distal to the scutellum was covered by a clear, strong signal (**Figure 6. D**, marked with yellow arrows). A confocal cross-section through a middle part of a bulge revealed its source (**Figure 6. D**, marked with dotted circles). It originated from the epidermal cells, which exhibited a pattern of signal distribution in which the fluorescent signal lined the cell membranes in contact with neighboring cells. Other sections of these proliferative bulges as well as the rest of the surrounding areas still contained some BdPIN1a-Citrine expression albeit on a weaker scale, such that it is not possible to determine where in them it appeared.

Following 72 hours of incubation on CIM and 24 hours after transfer to SIM (D1<sub>SIM</sub>), the switch becomes apparent at the level of PIN1a-Citrine presence. The transfer to SIM medium marks the switch from induction to maturation stage of SE. The explants experienced a global decrease in signal's intensity and it became limited only to bulging areas where its distribution pattern remained similar to that observed at D3<sub>CIM</sub> (**Supplemental Figure 1. E**, marked with dotted circles). Inside the bulges too, the signal pattern remained similar, albeit weaker. The membranous distribution visible at D3<sub>CIM</sub> appeared disturbed in comparison to the previous stage, although the previous distribution is still discernible to a point (**Figure 6. E**, marked with a dotted circle).

Observations of events after 48 hours on SIM (D2<sub>SIM</sub>) showed how *Bd*PIN1a-Citrine expression patterns did not change drastically with the bulges becoming more separated, becoming divided laterally from each other (**Supplemental figure 1. F**, arrows mark individual bulges). As for the fluorescent signal pattern, its presence spread to the whole of the bulge in most of objects (**Figure 6. F**). The pattern of a strong signal surrounding epidermal cells in contact with each other was reestablished (**Figure 6. F**, marked with a dotted circle) although with breakages consisting of multiple cells exhibiting such patterning (**Figure 6. F**, marked with arrows). The internal, subepidermal tissues of bulges were not marked by the signal.

After 72 hours of SIM (D3<sub>SIM</sub>), the zygotic embryos matured to a considerable point. The bulges have grown considerably and were 0.5 mm big with deep invaginations running across them (**Supplemental Figure 7. G**, marked with dotted circle). Root meristems began to appear in various stages of development inside the proliferative bulges (**Figure 6. G**, exemplary meristem marked with a yellow arrow). The forming meristems pointed inwards, towards the middle of the mass they grew from. Some of the less distinguishable meristems were connected with each other through tissue layers exhibiting a nonpolar distribution pattern of PIN1a-Citrine

(data not shown). Such meristems are marked with white arrows and a trace of the connecting tissue with a yellow dotted circle in **Figure 6. G**. Also, the proliferative bulge was partially covered with a strong epidermal signal akin to the same pattern as seen both at D3<sub>CIM</sub>, D1<sub>SIM</sub> and D2<sub>SIM</sub> (data not shown). A cross-section through a bulge containing this pattern is marked with dotted circles in **Figure 6. G** as well. Some root meristems fairly progressed with their development, making it possible to discern the future root cap and the root apical meristem (**Supplemental Figure 1. H**)

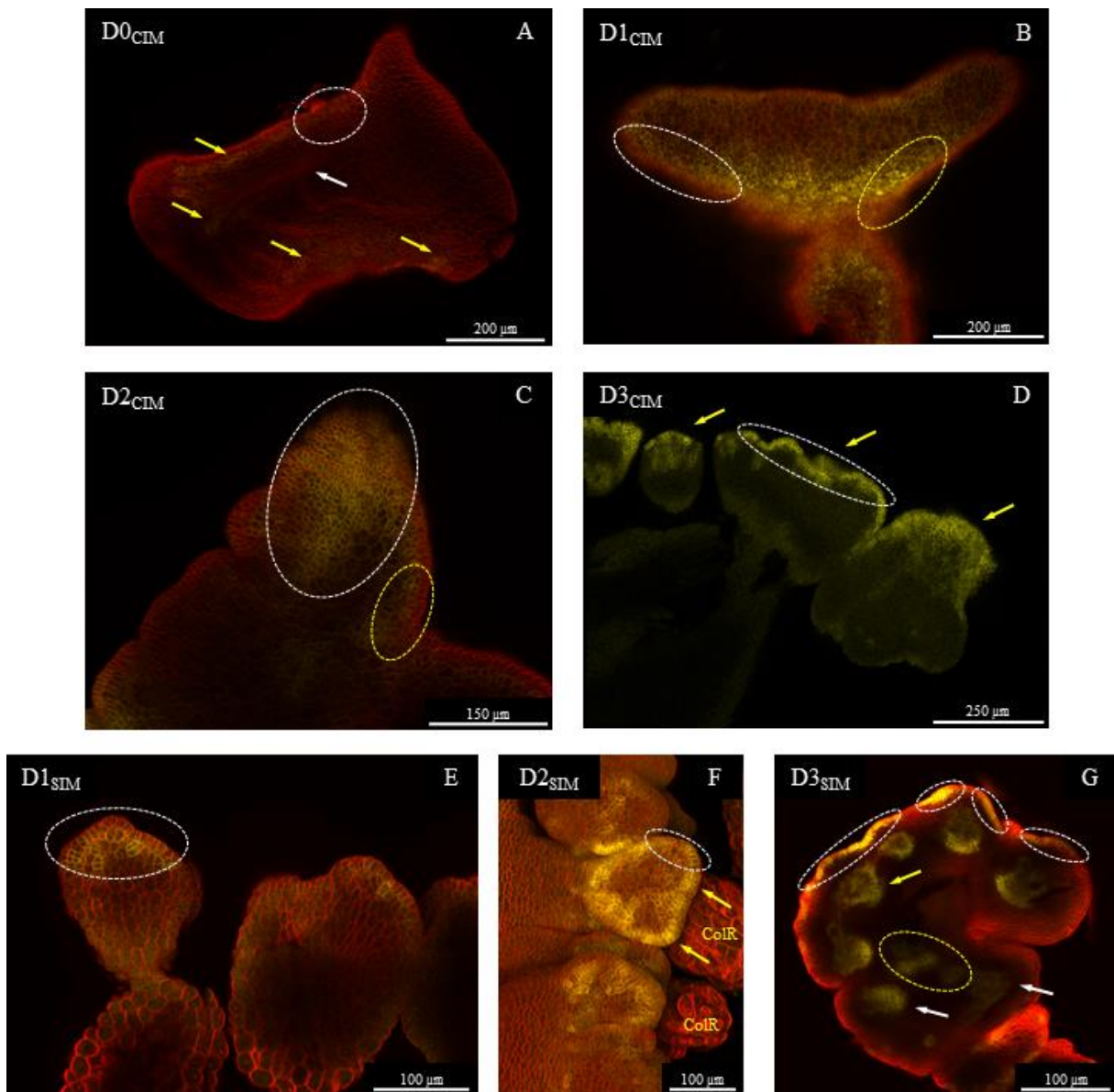


**Figure 6. Distribution patterns of PIN1a-Citrine during consecutive days of somatic embryogenesis.** PIN1a-Citrine signal is represented in yellow and the red signal represents the cell walls colored with Calcofluor White. *Continued on next page*



(A) Confocal cross-section through the scutellum of the zygotic embryo at D0<sub>CIM</sub>. Dotted circle marks the epidermal and parenchymal cell types that form it. Yellow arrows point to cell clusters adjacent to vascular tissues. White arrow marks the main vascular strand of the scutellum. (B) Confocal cross-section through the scutellum area opposite the coleorhiza at D1<sub>CIM</sub>. White dotted circle marks the parenchymal cells with a clear membranous signal. Yellow dotted circle marks the epidermal cell layer and parenchymal layer with diffuse signal present. (C) Confocal cross-section of the scutellum area where bulging took place at D3<sub>CIM</sub>. White dotted circle marks a newly present cell type inside the scutellum. Yellow dotted circle marks the epidermal and underlying parenchymal layer surrounding these new cells. (D) Confocal cross-section of recently formed proliferative bulges. Yellow arrows mark individual proliferative bulges. Dotted circle marks epidermal cells exhibiting a strong signal with a subcellular pattern of polarization. (E) Confocal cross-section of proliferative bulges at D1<sub>SIM</sub>. Dotted circle marks the area with peak signal intensity and remnants of distribution patterns from the previous stage of induction. (F) Maximum intensity projection of proliferative bulges at D2<sub>SIM</sub>. Dotted circle marks the reestablished pattern of PIN1a-Citrine in the epidermal cells. Arrows mark locations in the epidermis where that pattern of signal is broken. (G) Confocal cross-section of a proliferative bulge containing developing somatic embryos at D3<sub>SIM</sub>. Yellow arrow marks one developing root meristem in a progressive stage. White dotted circle marks residual epidermal presence of the fluorescent signal. White arrows mark root meristems in early developmental stages. Yellow dotted circle marks a trace of the tissue connecting the early-formed root meristems. *Abbreviations: D0<sub>CIM</sub> – D3<sub>CIM</sub> and D1<sub>SIM</sub> – D3<sub>SIM</sub> signify the length in days of consecutive explant incubation on callus- and shoot-inducing medium; colR – coleorhiza of the zygotic embryo*

## 4.2 Distribution of PIN1b, SoPIN1 and the transcriptional response to auxin during somatic embryogenesis

To sufficiently distinguish the onset of the three fluorescent signals before start of SE induction (D0<sub>CIM</sub>), a global view of the zygotic embryo was acquired (**Figure 7. A**). SoPIN1-Cerulean signal came from the cells forming the scutellum (**Figure 7. A1**, marked by a dotted circle), PIN1b-Citrine's from the ones forming the embryonic root tip (**Figure 7. A2**, marked by a dotted circle) and both signals partially overlapped in the shoot apical meristem (**Figure 7. A1 and A2**, marked by an arrow). Notably, both signals were also present in the rest of the embryo albeit with a low intensity that did not allow for pin-pointing of their source. The RFP signal originating from the DR5 auxin response reporter, although present globally on a weak scale, manifested the strongest in some of the cells appearing to originate from the surface of the scutellum, on the side opposite the embryonic shoot meristem (**Figure 7. A3**, marked by a dotted circle)

At D1<sub>CIM</sub>, the observed distribution patterns of the signals were different, their overlap having occurred in the surface tissue of the scutellum (**Figure 7. B**). SoPIN1-Cerulean was present there still, being exhibited by cells of the epidermal and the first few underlying parenchymal layers (**Figure 7. B1**). PIN1b-Citrine was at this point also visible in all the cells of the scutellum (**Figure 7. B2**). The RFP signal manifested solely in the surface cellular layers, although it was not intense enough to determine its accurate origin under low magnification used (**Figure 7. B3**). Overall, there was a higher density of RFP signal on the scutellum surface closer to the coleorhiza, as opposed to its presence on the other side of the scutellum at D0<sub>CIM</sub> (**Supplemental Figure 2. A, A1, A2 and A3**, which has the mentioned area marked with a dotted circle).

Stage D2<sub>CIM</sub> brought about the start of bulging, but no major shifts in fluorescent signal distribution occurred (**Figure 7. C**, bulging areas of the scutellum marked with a dotted circle). The overlap in fluorescent signal occurrence in cell types was again observed (**Figure 7. C1 and C2**) as was the low intensity of the RFP signal. The low intensity barred its accurate localization on a lower magnification, but nevertheless, its distribution appeared to be restricted to fewer surface cell layers than at previous stages (**Figure 7. C3**, areas marked with a dotted circle).

At D3<sub>CIM</sub>, proliferative bulges were detected and fluorescent signals exhibited novel distribution patterns. While proliferative bulges in advanced stages of development were not found, these novel patterns were still visible in some recently formed bulges (**Figure 7. D**, dotted circle marks the bulging area). SoPIN1-Cerulean exhibited peak intensity in the epidermal layer, revealing a polarization pattern in cellular membranes where neighboring cells touching each other are marked the strongest (**Figure 7. D1**, marked with a dotted circle). This pattern appeared interrupted at some locations in the bulge, where the signal intensity did not vary much in comparison to underlying cells (**Figure 7. D1**, marked with an arrow). As for PIN1b-Citrine, its peak intensity was manifested in the cellular clusters underneath the epidermal ones, with no membrane polarization pattern established (**Figure 7. D2**, marked with an arrow). The signal of RFP appeared further reduced when compared with its wide presence in the earlier stages and seems to be arranged in a way that certain cells with a stronger signal are surrounded with cells exhibiting a weaker one (**Figure 7. D3**). The cells exhibiting such patterns belong to the epidermis and the layers just underneath it. A broader perspective on these cellular events can be seen in **Supplemental Figure 8. B, 8. B1, 8. B2 and 8. B3**.

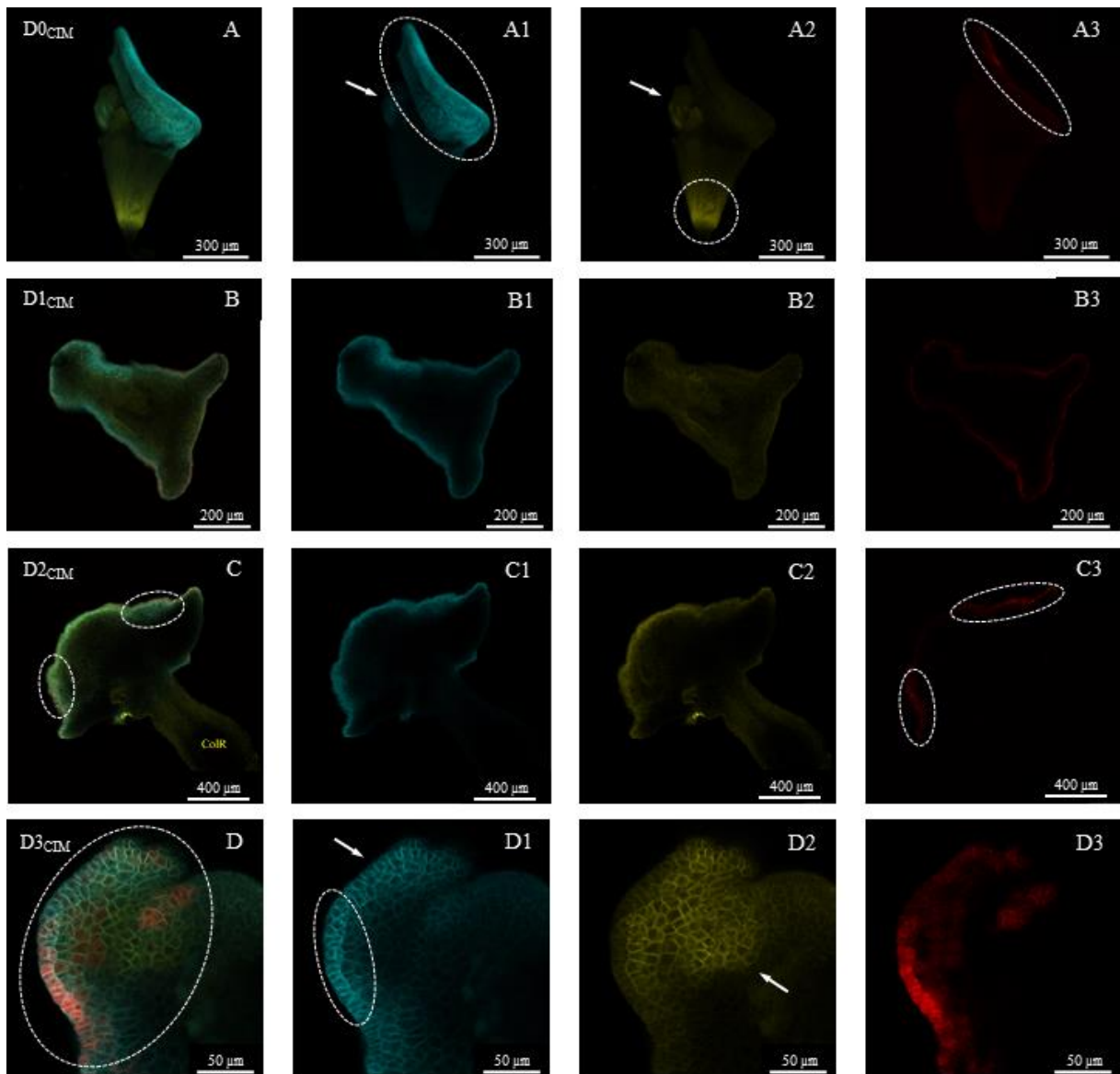


**Figure 7. Distribution patterns of SoPIN1-Cerulean, PIN1b-Citrine and presence of auxin tracked by DR5 transcriptional reporter during somatic embryogenesis.** First image of the series exhibits the overlay of the individual signal distributions throughout the same object. *BdSoPIN1*-Cerulean is shown in blue, *BdPIN1b*-Citrine in yellow and RFP expressed due to auxin presence in red. **(A)** Maximum intensity projection of the perspective on complete zygotic embryo seen from the sagittal plane at D0<sub>CIM</sub>. **(A1)** Dotted circle marks the scutellum while the arrow marks the shoot apical meristem. **(A2)** Dotted circle marks the embryonic root tip while the arrow marks the shoot apical meristem. **(A3)** Dotted circle marks the scutellum area where RFP is significantly present. **(B, B1, B2, B3)** Confocal cross-section of the scutellum at D1<sub>CIM</sub>. **(C, C1, C2)** Confocal cross-section of the complete zygotic embryo seen from the transversal plane at D2<sub>CIM</sub>. Dotted circles mark areas where bulging has started to occur. **(C3)** Dotted circle marks the area where RFP is significantly present. *Continued on next page*

**(D)** Confocal cross-section of a recently formed proliferative bulge at D3<sub>CIM</sub>. Dotted circle marks the bulge. **(D1)** Dotted circle marks the epidermal area where SoPIN1-Cerulean's signal peaks and exhibits a polar pattern of subcellular distribution. **(D2)** Arrow marks the subepidermal cell clusters marked strongly by PIN1b-Citrine. **(D3)** Distribution and presence of RFP. *Abbreviations: D0<sub>CIM</sub> – D3<sub>CIM</sub> and D1<sub>SIM</sub> – D3<sub>SIM</sub> signify the length in days of consecutive explant incubation on callus- and shoot-inducing medium.*

Once the switch to SIM has been made and D1<sub>SIM</sub> stage was reached, the signal in the bulging areas was visibly affected (**Figure 8. A**, marked by a dotted circle). Both SoPIN1-Cerulean and PIN1b-Citrine signals became diffuse and weak in intensity and their localization could not be determined (**Figure 8. A1 and A2**). The RFP signal experienced a similar change, although its localization still could be pin-pointed to individual cells (**Figure 8. A3**, marked by a dotted circle).

Reaching the D2<sub>SIM</sub> stage, the bulging masses have grown significantly (**Figure 8. B**, bulges marked with a dotted circle) and the pattern of exclusive complementarity of SoPIN1-Cerulean and PIN1b-Citrine signals began to be apparent again (**Figure 8. B1 and 8. B2, Supplemental Figure 3. A, A1 and A2**). A novel pattern of was exhibited by the RFP signal, being almost absent from the proliferative bulges and present in their surroundings (**Figure 8. B3**).

At D3<sub>SIM</sub>, some signal distribution patterns already seen during previous stages were detected again (**Supplemental Figure 3. B series** exhibiting a proliferative bulge in early development and **Supplemental Figure 3. C series** exhibiting a proliferative bulge in a progressive stage with the RFP signal gone) along with forming somatic embryos containing some mature embryonic tissues (**Figure 8. C and Supplemental Figure 4. A and B**). Depending on the developmental progress, embryonic roots with a root cap (**Figure 8. C2**, marked with white arrows) or root stele (**Supplemental Figure 4. A1**, marked with a dotted circle) strongly marked by PIN1b-Citrine were visible as was an embryonic shoot, marked strongly by SoPIN1-Cerulean (**Supplemental Figure 4. B2**, marked with a dotted circle). In all of these objects there was some SoPIN1-Cerulean signal present in the epidermal and the underlying layers, although less in tissues that progressed further in embryogenesis. An absence of the RFP signal was apparent in most of detected and examined objects although it was still present globally, except from the more embryogenetically developed tissues (data not shown).

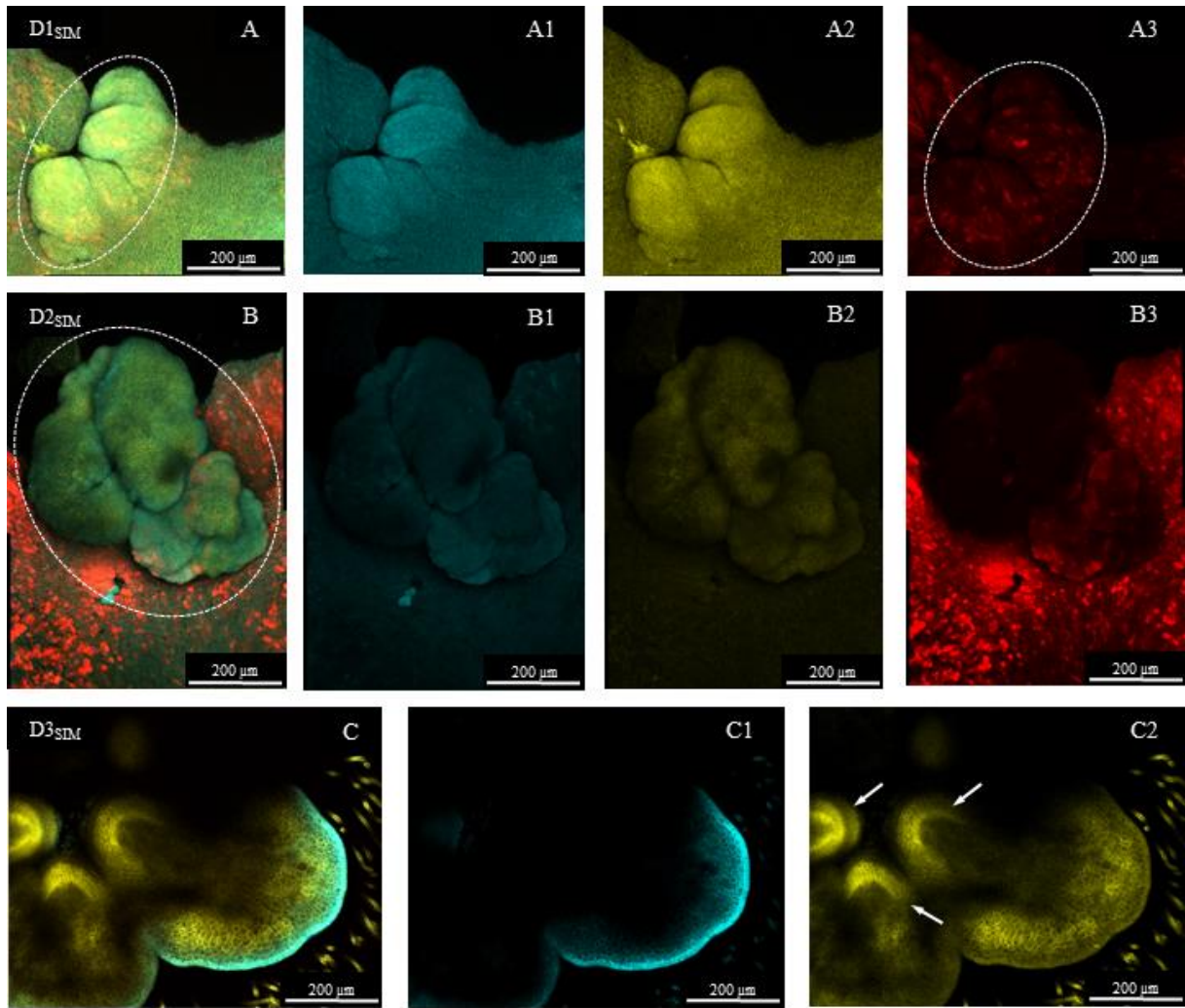


**Figure 8. Distribution patterns of SoPIN1-Cerulean, PIN1b-Citrine and presence of auxin tracked by DR5 transcriptional reporter during somatic embryogenesis.** First image of the series exhibits the overlay of the individual signal distributions throughout the same object. *BdSoPIN1*-Cerulean is shown in blue, *BdPIN1b*-Citrine in yellow and RFP expressed due to auxin presence in red. (A, A1, A2) Maximum intensity projection of fluorescent signals in the proliferative bulges at D3<sub>SIM</sub>. Dotted circle marks the proliferative bulges. (A3) Dotted circle marks the area of the bulges where RFP is significantly present. (B, B1, B2, B3) Maximum intensity projections of signal in the proliferative bulges at D2<sub>SIM</sub>. Dotted circle marks the bulges (C, C1, C2) Confocal cross-section of the complete zygotic embryo seen from the transversal plane at D3<sub>SIM</sub>. (C2) Arrows mark forming embryonic root caps. Abbreviations: D0<sub>CIM</sub> – D3<sub>CIM</sub> and D1<sub>SIM</sub> – D3<sub>SIM</sub> signify the length in days of consecutive explant incubation on callus- and shoot-inducing medium.

### 4.3 Presence of auxin tracked with the DII-VENUS during somatic embryogenesis

The degraon-based, constitutively expressed reporter of auxin DII-VENUS was used to track auxin presence. This reporter was designed for degradation of fluorescent protein VENUS to occur when it comes in contact with auxin. Although planned, results were not obtained for induction on SIM due to a lack of response in the explants, due to technical difficulties with cultivation.

Before incubation, the VENUS signal was present in both the epidermal and inner parenchymal cells of the scutellum (**Figure 9. A**, showing a confocal cross-section through the scutellum). At D1<sub>CIM</sub>, the overall intensity of the signal in all cell layers was significantly lower, although it did not disappear completely (**Figure 9. B** and **C**). The signal continues to diminish globally during D2<sub>CIM</sub> stage as well. Bulge formation has taken place at this point (**Figure 9. D**, marked with a dotted circle) and the bulges mostly do not contain any signal inside them (**Figure 9. E**, marked with a dotted circle). Internally in the embryo, the presence of signal was still visible in the tissue areas farther away from the developing bulges (**Figure 9. E**, marked with an arrow). At the D3<sub>CIM</sub> stage, a shift in signal distribution has occurred with VENUS becoming absent in the scutellum tissues surrounding the bulges while simultaneously marking the bulges themselves (**Figure 9. F**, part of bulges marked with a dotted circle). Moreover, the signal seems to be stronger closer to the epidermal layers of the bulges and more or less inexistent in the inner tissues (**Figure 9. G**).

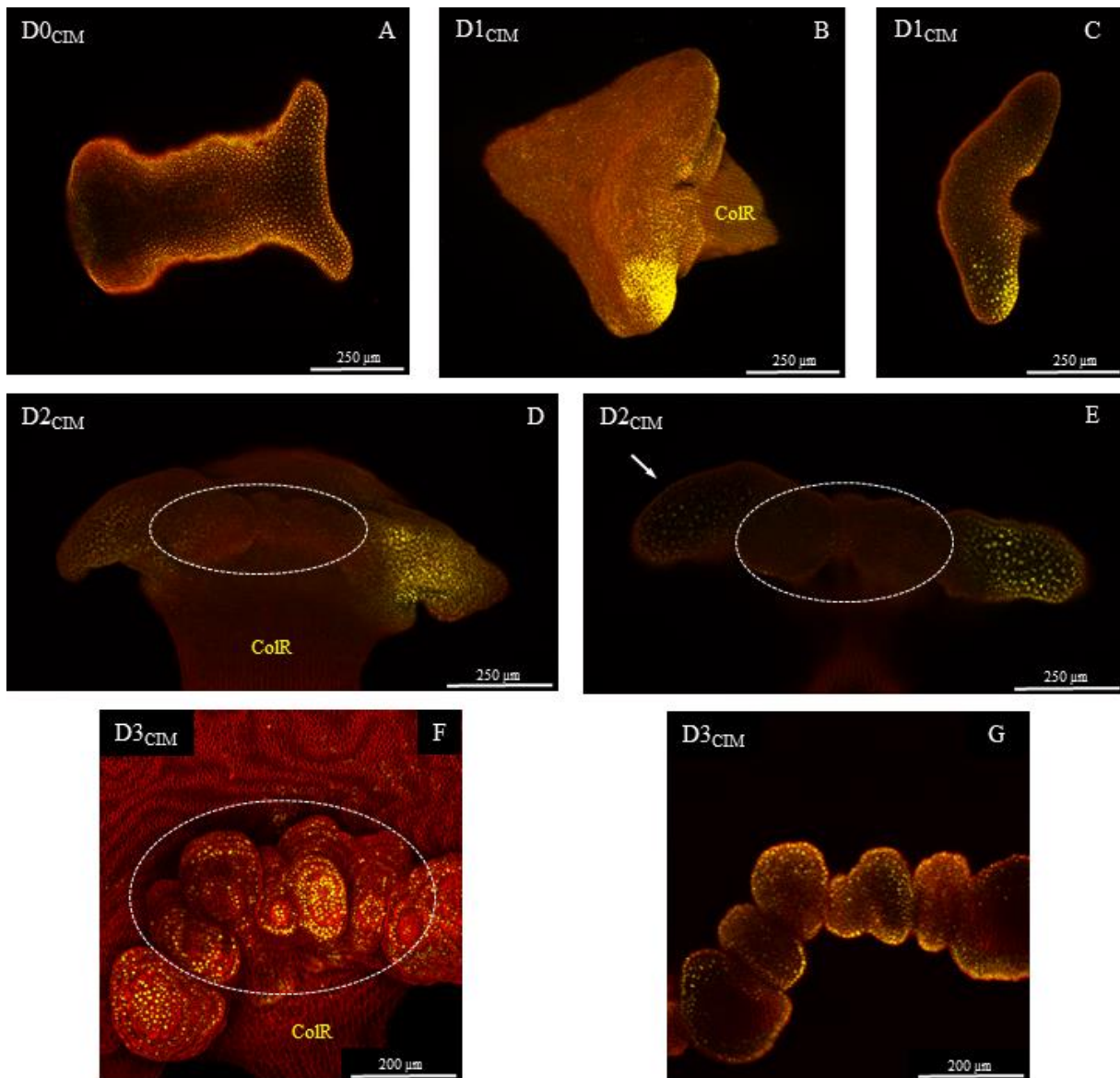


**Figure 9. Distribution of auxin during somatic embryogenesis, tracked with the DII-VENUS auxin reporter, degraded in presence of auxin.** VENUS is shown in yellow and the red signal represents the cell walls colored with Calcofluor White. **(A)** Confocal cross-section of the scutellum of a zygotic embryo at D0<sub>CIM</sub>. **(B)** Maximum intensity projection of signal presence in the scutellum seen from the transverse plane at D1<sub>CIM</sub>. **(C)** Confocal cross-section through the scutellum from the transverse plane at D1<sub>CIM</sub>. **(D)** Maximum intensity projection of signal presence in the scutellum seen from the transverse plane at D2<sub>CIM</sub>. Dotted circle marks the forming proliferative bulges **(E)** Confocal cross-section of the scutellum seen from the transverse plane at D2<sub>CIM</sub>. Dotted circle marks the forming proliferative bulges. Arrow marks the area away from the bulges with VENUS still present. **(F)** Maximum intensity projection of signal presence in the proliferative bulges at D3<sub>CIM</sub>. Dotted circle marks some of the proliferative bulges. **(G)** Confocal cross-section of proliferative bulges at D3<sub>CIM</sub>. *Abbreviations: D0<sub>CIM</sub> – D3<sub>CIM</sub> and D1<sub>SIM</sub> – D3<sub>SIM</sub> signify the length in days of consecutive explant incubation on callus- and shoot-inducing medium. colR – coleorhiza.*



#### 4.4 Comparison of tissue sections of *B. distachyon pin* loss-of-function mutant explants undergoing somatic embryogenesis

For the purpose of identifying whether major phenotypic differences exist among the three available loss-of-function mutants, *B. distachyon* zygotic embryos were examined at the D3<sub>CIM</sub> and D3<sub>SIM</sub> stages utilizing PAS/NBB staining and compared to wild-type explants. No reacting *pin1a* loss-of-function explants were produced at D3<sub>CIM</sub>, unfortunately.

A cross-section through the transversal plane of a *pin1a* × *pin1b* zygotic embryo at D3<sub>CIM</sub> revealed the various tissues that comprise it, which could roughly be divided into the epidermal layers and the inner parenchymal cells (**Figure 10. A**, with the position of the main vascular strand of the embryo and the scutellum area of interest indicated). Based on the PAS/NBB staining, the scutellum area where bulging took place could be divided into three more or less distinct cell populations. The epidermal layer stood out with its total dark blue coloration. The underlying subepidermal layer's cell content stained both blue and pink while the layer underneath it stained prevalently pink, apart from the cell walls. Clear boundaries between the layers could not be outlined, but the continuum of histological differences occurring was overall apparent (**Figure 10. B**).

As for the *pin1b* explant, a view of the developing proliferative bulges was captured from the same plane (**Figure 10. C**). The growth of bulges appeared to have progressed more compared to the *pin1a* × *pin1b* explant but still three cellular layers were visible (**Figure 10. D**, yellow arrows mark proliferative bulges). The epidermal and the inner layer of starch containing cells did not seem strikingly different, however, the subepidermal layer was not stained as pink as it did in the previously examined explant.

A transversal cut was obtained for the wild-type explant too (**Figure 10. E**). Focusing on the area of interest, a similar histologic pattern as in the *pin1b* explant was visible, as well as the bulge growth progress (**Figure 10. F**, dotted circle marks the growing proliferative bulges). The dark blue epidermal cells were present on top of the blue subepidermal cells, while under them, the pink stained layer was located.



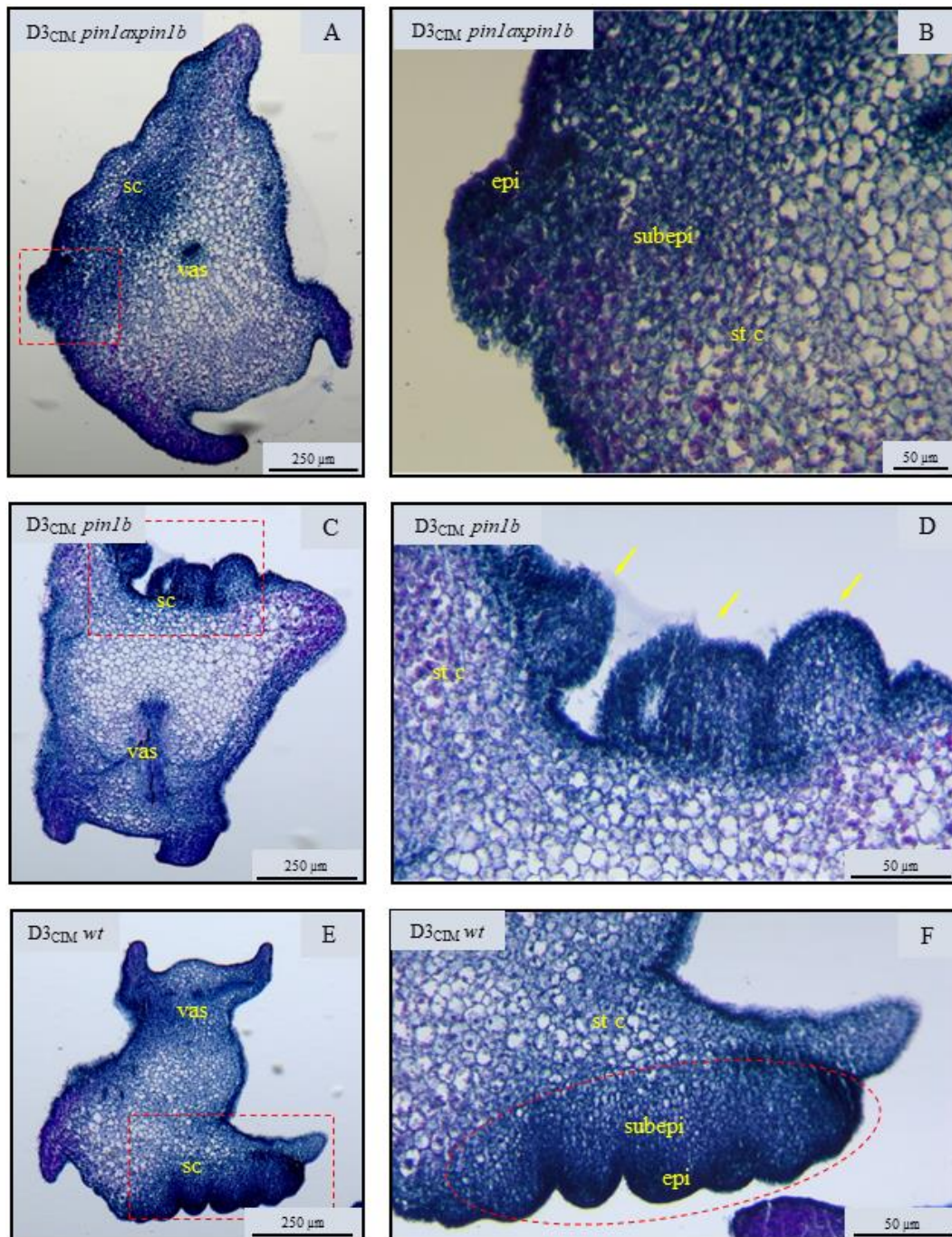


**Figure 10. Histological patterns in the *pin1a* × *pin1b* and *pin1b* loss-of-function mutants in comparison to a wild-type explant at D3<sub>CIM</sub>.** Naphtol Blue Black dyes proteins in blue and cell nuclei in dark blue while Periodic Acid Schiff dyes polysaccharides in pink. (A1, B1, C1) Transversal cross-sections of zygotic embryos. (A2) Close-up of the transversal cross-section A revealing cellular structure of the scutellum tissue. (B2) Close-up of the transversal cross-section C revealing forming proliferative bulges. (C2) Close-up of the transversal cross-section E revealing many forming proliferative bulges. Abbreviations: D0<sub>CIM</sub> – D3<sub>CIM</sub> and D1<sub>SIM</sub> – D3<sub>SIM</sub> signify the length in days of consecutive explant incubation on callus- and shoot-inducing medium. sc – scutellum, vas – vasculature, epi – epidermis, subepi – subepidermis, st c – starch rich cells.

Reaching the D3<sub>SIM</sub> stage, developmental progress was visible in the explants. A sagittal cross-section through the *pin1a* × *pin1b* explant revealed the presence of late-stage proliferative bulges that likely represent proembryogenic masses (**Figure 10. A**). These cellular structures are marked with deep blue coloration that was present in two hues, one marking a few surface layers and the other marking the layers underneath, inside the structures (**Figure 10. B**). A similar pattern was visible in both the *pin1b* (**Figure 10. C and D**) and *pin1a* explants (**10. E**). On the other hand, the wild-type explant at D3<sub>SIM</sub> stage has again developed significantly more compared to the loss-of-function mutants. While also exhibiting similar coloration patterns in the embryogenic tissues, among the proembryogenic masses of considerable size it contained, a distinctly developed somatic embryo with a mature shoot was even detected (**Figure 10. F**, dotted square marks the somatic embryo).

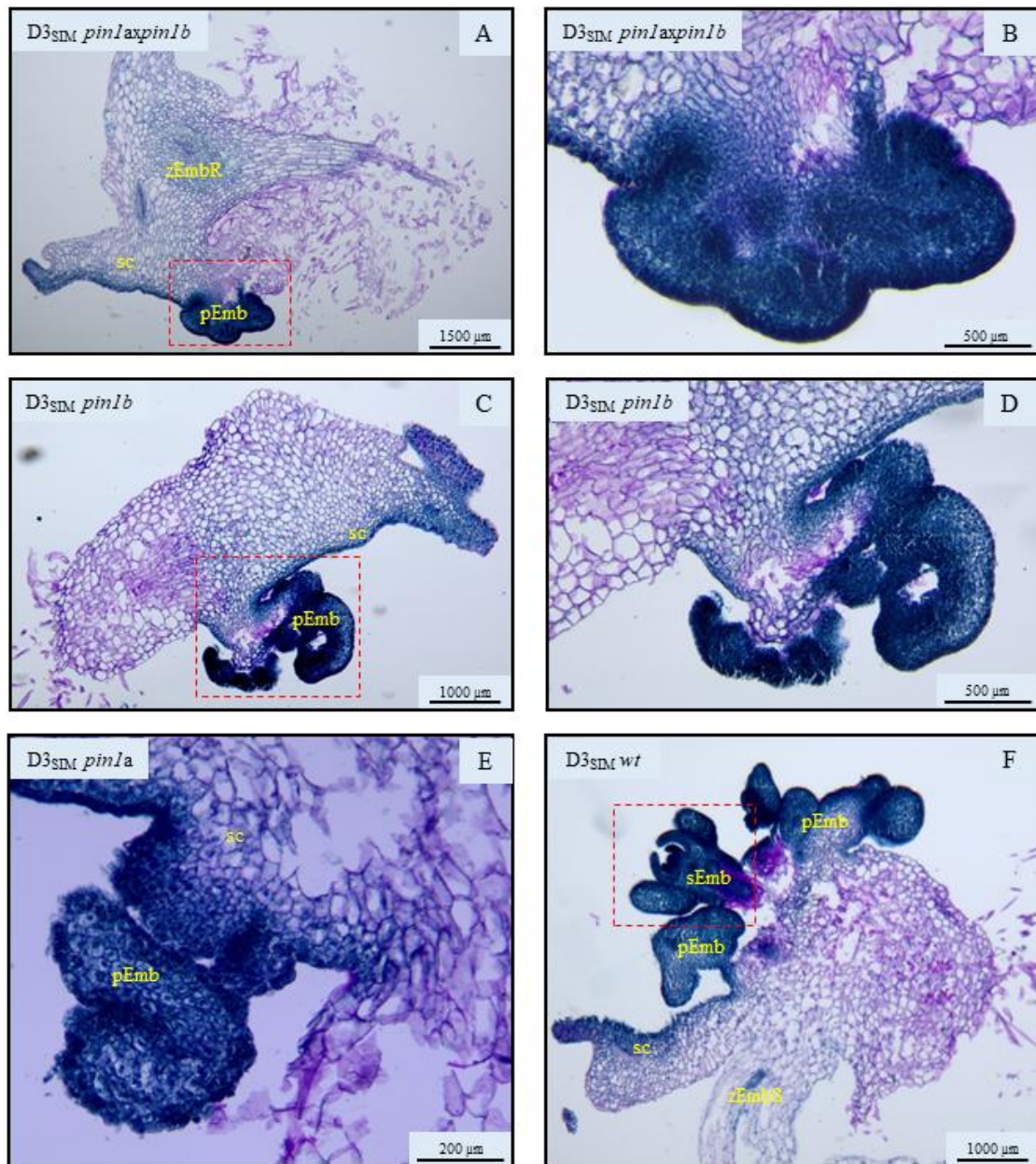


**Figure 11. Histological patterns in the *pin1axpin1b*, *pin1b* and *pin1a* loss-of-function mutants in comparison to a wild-type explant at D3SIM.** Naphtol Blue Black dyes proteins in blue and cell nuclei in dark blue while Periodic Acid Schiff dyes polysaccharides in pink. (A, C) Sagittal cross-sections of zygotic embryos with visible proembryogenic masses. (B, D) Close-ups of the sagittal cross-sections A1 and B1 revealing the developing proembryogenic masses up-close. (E) Close-up of a developing proembryogenic mass. (F) Sagittal cross-section of a zygotic embryo containing proembryogenic masses along with a developed somatic embryo. *Abbreviations: D0<sub>CIM</sub> – D3<sub>CIM</sub> and D1<sub>SIM</sub> – D3<sub>SIM</sub> signify the length in days of consecutive explant incubation on callus- and shoot-inducing medium. sc – scutellum, zEmbR – zygotic embryo root, pEmb – proembryogenic mass, sEmb – somatic embryo, zEmbS – zygotic embryo shoot.*



## 5. DISCUSSION

---

### 5.1 Occurrence of PIN1a in somatic embryogenesis of *B. distachyon*

Findings presented here confirmed *BdPIN1a* to be expressed continuously throughout somatic embryogenesis. In spite of this, the determination of its role and how it shapes sEMB formation could not be determined with certainty. Many distribution patterns of *BdPIN1a* during SE were detected and the basis of their interpretation is the notion that what is being observed are snap-shots of a dynamic process. To be more exact, four distinct major distribution patterns could be singled-out in presented results, with the rest presumably being intermediary stages between two distinct ones. First one was detected at D2<sub>CIM</sub>, when PIN1a patterned membranes of small, irregularly shaped cells inside the scutellum in a nonpolar fashion (**Figure 6. C**). Second one is exemplified at D3<sub>CIM</sub> where PIN1a covered the part of the proembryogenic mass positioned distally from the scutellum and where it was exhibited by the epidermal layer, lining their membranes where they touched neighboring cells (**Figure 6. D**). The third distribution pattern arose at D2<sub>SIM</sub>, where the complete epidermis of a developing somatic embryo contained PIN1a in neighboring cells that were in contact (**Figure 6. F**). The fourth pattern was visible at D3<sub>SIM</sub> in sEMBs where PIN1a marked root meristems (**Figure 6. G**). The nature of these tissues was determined to be of root meristem due to its visual similarity to its expression pattern in non-treated explants (data not shown). This suggests that, as the sEMBs mature, PIN1a possibly starts to take up its physiological role.

Presence of *BdPIN1a* in SE was previously observed macroscopically and it was found that its expression coincides with embryogenic areas of callus, starting from the third and continuing to the 28<sup>th</sup> day on CIM (Wehbi 2020). Furthermore, the same publication demonstrates that *PIN1a* expression coincides with expression of *WOX11* of *B. distachyon*, a member of the WUSCHEL homeobox-containing (WOX) protein family that is involved in many specialized functions in plant development (van der Graaff et al. 2009). *BdWOX11* is among 2 of the 13 *WOX* genes of *B. distachyon*, unique due to its continuous expression through the starting period of SE induction (Wehbi 2020). Wehbi demonstrates that the two genes overlap in their expression inside the proliferative bulges forming on the scutellum, albeit in separate zones. At D3<sub>CIM</sub> *BdPIN1a* is expressed abundantly in the upper layers of the bulges while *BdWOX11* is present mostly inside the layers, underneath the epidermal surface. These *in situ* hybridization results of *PIN1a* expression detection resemble patterns I observed during

D2<sub>CIM</sub> stage (**Supplemental Figure 1. C**). This co-occurrence of expression in *PIN1a* and member of the *WOX* gene family further implicates *PIN1a* as an important player in SE.

Drawing functional parallels between *BdPIN1a* and PIN transporters of other species is unfortunately not a completely viable way to speculate on its function. Functions cannot be compared reliably to the main model of plant science either, as *A. thaliana* PIN1 has gained the uncommon ability to mediate both convergent polarization patterns and organ initiation through canalization of auxin (O'Connor et al. 2017). Such a duality in function of *PIN1a* is unique to the *Brassicaceae* while in the majority of angiosperms, these two functions are taken up not only by PIN1 but also other PINs including SoPIN1 family of transporters (O'Connor et al. 2017). No meaningful comparisons can be made with maize or rice, as both species contain four variants of PIN1 (Wang et al. 2009; Forestan et al. 2012) and little or no relevant information is currently available on the way they affect auxin flow during somatic embryogenesis. No available data on other species of the genus *Poaceae* exists either. Nevertheless, a valuable study (O'Connor et al. 2014). on *PIN1a* function was undertaken on its role in spikelet initiation in *B. distachyon*. It was found to be expressed in the corpus of the shoot meristem, along with *PIN1b*, where it polarized away from convergent points of auxin. This pattern was consistent with the with-the-flux model of polar auxin transport (PAT), acting to induce canalization of auxin through development of vascular tissue tracks (O'Connor et al. 2014). Study of occurrence of *BdPIN1a* in zygotic development supports that its functions remains similar in other developmental processes. Hao et al. (2021) detected *BdPIN1a* presence continuously through zygotic embryogenesis and it appeared to occur in correlation to vascular tissues of the zEMB during its later developmental stages. *BdPIN1a* was detected during early stages of embryogenesis, being present in the top inner cells of the proembryogenic mass, but this finding is hard to correlate with results presented here, as patterns similar to this were not observed. Data presented by Hao et al. (2021) reveal early developmental patterns that are hard to correlate with early events of SE in light of available data presented in this publication. On the other hand, their data on the late developmental stages of the zygotic embryo coincide with what was detected in the zygotic embryo at D0<sub>CIM</sub> (data not presented), pointing not only to both similarities and differences in development of somatic and zygotic embryos but also to a hole in the dataset that has to be explored as a standalone topic.

Evidently, *BdPIN1a* did not match the patterns it displays during spikelet initiation in the shoot meristem or zygotic development, its distribution patterns being more varied or entirely different during SE. The main notable difference is that its distribution aligns more

with the concentration-based model of PIN distribution forming PAT as opposed to the patterning present during spikelet formation in the shoot meristem, where PIN1a distribution can be interpreted through the flux-based model. This difference is most likely connected to the different expression patterns observed for PIN1a, it being present in inner tissues of the shoot meristem during spikelet initiation and epidermally in developing somatic embryos throughout SE. Nevertheless, having in mind the conclusions on PIN1a being involved in canalization of auxin away from convergent points i.e. local auxin maxima and presented by O'Connor et al. (2014), a theory on the way it shapes auxin flux can be constructed. The first distribution pattern could be attributed to a global and nonselective rise in PIN expression that is known to occur after tissues are exposed to auxin (Křeček et al. 2009). SE continues to progress and PIN1a is displayed in epidermal distribution patterns on contact surfaces between neighboring cells. First it occurs partially as in the second, and then globally as in the third distribution pattern. It could potentially act there to siphon auxin from the epidermal layer into the inner tissues of the developing somatic embryos. The origin of the auxin could be the epidermal layer itself, as a jump start in its biosynthesis following induction using 2,4-D is known to occur (Elhiti et al. 2010; Liao et al. 2015). Finally, after reaching the maturation phase of SE, PIN1a takes up its physiological role in embryo development. Future examinations should aim to build upon or disprove this model. Most valuable data could be gathered by developing lines carrying both the fluorescently-tagged PIN1a along with a marker of auxin such as DR5. This would allow localization of local auxin maxima and could explain how PIN1a distribution patterns relate to auxin flux. Another important point for future reference would be the discrepancy in PIN1a expression patterns in the developmental processes where its function was studied so far.

## 5.2 Occurrence of PIN1b and SoPIN1 in somatic embryogenesis of *B. distachyon*

Tracking the expression patterns of PIN1b and SoPIN1 revealed them to be generally simpler than the ones observed for PIN1a, not changing drastically throughout SE. As I observed PIN1b and SoPIN1 jointly, their patterns of distribution will be summarized in relation to one another. The distribution patterns of these PINs are interpreted in light of results presenting snapshots of a developmental process as well. I propose that three major patterns can be distinguished, with a major turning point between the first two occurring at D2<sub>CIM</sub>. Before this point, PIN1b and SoPIN1 expression coincides in all the scutellum cells (**Figure 7. B**). After D2<sub>CIM</sub>, PIN1b begins to be expressed in the inner tissues of proliferative bulges and

the scutellum while SoPIN1 is restricted to their epidermis (**Figure 7. D, Supplemental Figure 2. B**). At D3<sub>SIM</sub> mature somatic embryos were noticed and as did PIN1a, both PIN1b and SoPIN1 seem to take up their physiological distribution there (**Figure 8. C and Supplemental Figure 4. A and B**).

Wehbi (2020) determined how PIN1b coincides with subepidermal layers in regions of embryogenic callus, starting to be distinctly noticeable after three days on CIM. Wehbi explored the expression of SoPIN1 macroscopically as well, detecting its presence during the first eight days on CIM and then disappearing until the 22<sup>nd</sup> day on CIM, coinciding as well with embryogenic zones.

PIN1b and SoPIN1 are among the PIN transporters whose function is explored in spikelet development of *B. distachyon* (O'Connor et al. 2014) and through heterologous expression in *A. thaliana pin1* knockout mutants (O'Connor et al. 2017). PIN1b was, similarly to PIN1a, expressed in the corpus of the shoot meristem but in a much broader manner and with weaker relative intensity. It is theorized that such a widespread and weakly expressed pattern acts to create broad regions of auxin flux towards the sink (reviewed by O'Connor et al. 2014). O'Connor et al. demonstrated through observations of PIN1b presence in the meristem coupled with computational modeling that its function is creation of broad PAT areas through which auxin is channeled and which connect to and develop into vascular tissues.

As for SoPIN1, it was found to be expressed in the tunica of the shoot meristem where it created auxin convergence points i.e. local auxin maxima at sites where organ initiation occurs afterwards (O'Connor et al. 2014). Furthermore, members of the SoPIN1 family were studied in *Solanum lycopersicum* (L.) and *Medicago truncatula* (Gaertn.) where they also play a role in formation of epidermal auxin maxima that leads to organ initiation (reviewed by O'Connor et al. 2017), further supporting that it functions in such a fashion in *B. distachyon* as well. Interestingly, *BdSoPIN1* expressed under native promoters of *AtPIN1* was found to be able to rescue organ initiation in *Atpin1* mutants while *BdPIN1b* under the same promoter in the same mutant could not (O'Connor et al. 2017). If convergence of auxin is critical for SE initiation, SoPIN1 evidently would play a crucial role in it.

In the study of Hao et al. (2021) that examined among other things the presence of selected *BdPIN1s* during zygotic embryogenesis, PIN1b correlated with presence of PIN1a in the inner cells of the embryo during all stages of zygotic embryogenesis, albeit with a broader distribution pattern. Both *BdPIN1s* occurred near the vasculature but in a pattern concordant

with their presumed functions described by O'Connor et al. (2014) and O'Connor et al. (2017). SoPIN1 was detected in or near the epidermal cells of a developing zygotic embryo early and then associated more with the cells of the scutellum and the shoot meristem later on. As noted for PIN1a, these observations for PIN1b and SoPIN1 are very similar to distribution patterns I detected at D0<sub>CIM</sub> (data not shown) while not resembling anything detected during SE itself. These patterns confirm that PIN1b and SoPIN1 could potentially have a similar function in many developmental processes. Again, similarly to PIN1a, the data available on distribution of PIN1b and SoPIN1 in zygotic tissues does not reveal what their exact physiological role is either. Data presented in Hao et al. (2021) reveal early developmental patterns that are hard to correlate with early events of SE, in light of the presented data yet coincide with what was detected at D0<sub>CIM</sub> in my work (data not presented), pointing to correlations in development of embryos but also to a topic for future study.

Having in mind these findings on SoPIN1's and PIN1b's function and the fact that their distribution presented here aligned with the previous findings on their polar distribution patterns which create auxin flux (O'Connor et al. 2014; O'Connor et al. 2017), I propose the following sequence of events occurs during SE in *B. distachyon*. I would ascribe their first distribution pattern to a global and nonselective rise in PIN expression that is known to occur after tissues are exposed to auxin (Křeček et al. 2009). As the second pattern is marked by an appearance of an excluding but complimentary expression zones, I suggest that SoPIN1 acts to create auxin maxima in the epidermal cells that are producing endogenous auxin as an effect of 2,4-D induction. I suspect these local auxin maxima induce the developmental shift in one or more cells that start to divide and build the proliferative bulges. As this is occurring, PIN1b acts to siphon the auxin from there to inner scutellum tissues, away from the proliferative bulges thus creating a flux that shapes the developmental changes. Finally, after reaching the maturation phase of SE, both PINs take up their physiological roles and display the third distribution pattern. As for their physiological distributions presented in Hao et al. (2021), as was the situation for PIN1a, the early ones are hard to correlate with patterns detected during SE while the later ones clearly resemble immature zygotic embryos at D0<sub>CIM</sub>.

### 5.3 The occurrence and flow of auxin during somatic embryogenesis of *B. distachyon*

DR5, the synthetic transcriptional reporter driving expression of RFP as a part of an auxin-related transcriptional response (O'Connor et al. 2014) and the degron-based reporter DII-VENUS which reveals presence of cellular auxin through degradation of the VENUS



fluorescent marker (Brunoud et al. 2012) were utilized to determine how and where is auxin localized during somatic embryogenesis of *B. distachyon*. This way, the utilization of two auxin trackers could provide a stronger evidence upon which a hypothesis could be formed. Unfortunately, the DII-VENUS data for SIM stage was not utilized due to a lacking growth response of mother plants that manifested in non-responding zEMB explants. Because of this, interpretations of the SIM stage are based solely on the DR5 marker. Nevertheless, a hypothesis on auxin occurrence and global flow can be reconstructed.

Similarly to observed PINs, patterns of RFP expression and degradation of VENUS indicating presence of auxin change during stages of SE and their major distribution patterns can be identified as well. Starting with observations of DR5-driven expression of RFP, its initially global epidermal expression becomes limited to an epidermal scutellum area opposite the coleorhiza, where proliferative bulges are found to form later on, as is described by Wehbi et al. (2022). Second, at D3<sub>CIM</sub>, RFP is expressed in the epidermal layers surrounding proliferative bulges. RFP is weak or not present inside the bulges themselves. This pattern continues to evolve during SIM, the more the embryogenic tissues develop into somatic embryos, the less RFP is expressed in their epidermis while still being expressed in the surrounding scutellum cells where SE is not occurring.

The theory I would like to suggest is supported by observations presented by Benkova et al. (2003), where it is postulated that local, efflux-dependent auxin gradients are a common module for organ development. As it is likely that the underlying molecular mechanisms are shared among higher plants, this model has a potential to be generalized. Interpreting early stages of SE in *B. distachyon* in this way leads to the following interpretation. During the stage where proliferative bulges form, a connection still exists with the underlying mother tissue, a connection that could enable efflux from epidermal auxin convergence points. Based on this, I suggest that before D3<sub>CIM</sub> and appearance of proliferative bulges, local auxin maxima are formed in the epidermis of the scutellum and this results in developmental reprogramming of certain cells which essentially initiates SE. Illustration of this was observed and documented in **Figure 7. D3**. This is further indirectly supported by study on SE done on *A. thaliana* in which the establishment of auxin gradients in specific regions of embryogenic callus correlates first with expression of *WUS* and the appearance of somatic embryos (Su et al. 2009). The activity of *ARFs* monitored in *A. thaliana* zEMBs during SE through GFP-tagging also correlates strongly with SE induction (Wójcikowska & Gaj 2017).

As for the DII-VENUS carrying explants and their response to CIM, only conclusions from a broad histological perspective can be made due to a lack of observed SE-related cellular events. Nevertheless, the tissue-level observations indirectly support the presented theory as distribution patterns of VENUS both confirm and build upon statements made on the basis of DR5-driven RFP expression. Global presence of VENUS drops the longer the incubation takes place, starting from  $D0_{CIM}$  and up to  $D2_{CIM}$ . One exception to this pattern, visible in **Figure 9. B, C, D and E**, is a persistent VENUS signal in one part of the scutellum, suggesting that there is no auxin. This zone actually does not react to auxin as during the response of the immature zEMB to CIM, its expanding coleoptile and coleorhiza push one side of the scutellum into the medium, placing the other side away from it. Continuing on, at  $D3_{CIM}$  stage VENUS is present in epidermal cells of the proliferative bulges and nowhere else (**Figure 9. F and G**). I suggest that an efflux of auxin occurs from the proliferative bulges, passing through their inner tissues and flowing towards the scutellum while not even affecting their epidermal layers.

I theorize that efflux of auxin from the embryogenic tissues towards the mother-tissues of the scutellum continues to occur during SIM (**Figure 8. B3**) and induces SE in surrounding tissues *de novo*. This statement is supported by detection of distribution patterns of PINs and auxin at  $D3_{SIM}$  that were already found at stages of CIM (**Supplemental Figure 3. B and C**). Such histological patterns are in stark contrast to somatic embryos that are also detected at this stage (**Supplemental Figure 4.**). I suspect the reason behind is that endogenous auxin siphoned from proliferative bulges that were induced to SE, using exogenous auxin contained in CIM, induces similar changes in the rest of the scutellum cells that are still inductive to SE. This flux does not affect somatic embryos any more in their maturation phase, considering that their meristems are separated from mother-tissue they arose from, due to development of their own vasculature. This separation is regarded as a critical step in SE, with studies suggesting that embryonic development of shoot and sEMBs represents a developmental continuum dependent on auxin concentration. The difference in auxin concentration is linked to a lack or existence of connection with mother-tissues that acts as auxin sinks (Elhiti & Stasola 2022). While such a connection evidently exists during early stages of *B. distachyon* SE, it is not clear when and how it becomes severed, but evidently sometimes during SIM incubation and before  $D3_{SIM}$  stage. Data on DII-VENUS carrying explants during SIM as well as more detailed studies of cellular events could surely shed more light on this aspect of SE.

#### 5.4 Histological traits of PAS/NBB stained loss-of-function mutants *pin1a*, *pin1b* and *pin1a* × *pin1b* of *B. distachyon*

Phenotypic differences that manifested in a delay in SE were detected in *B. distachyon* cross-sections of loss-of-function mutants *pin1a*, *pin1b* and *pin1a* × *pin1b*, when compared to the wild-type explant, both at the D3<sub>CIM</sub> and D3<sub>SIM</sub> stage. In spite of this, no visual histological differences have been detected in the PAS/NBB stained cross-sections of the explants, likely due to the well-known functional redundancy of PIN auxin transporters (Křeček et al. 2009) which allows the developmental events to continue. Furthermore, all explant types exhibited some histological similarities regardless of their impediment in SE progression.

The scutellum of all D3<sub>CIM</sub> explants consisted of similar cellular types but the developmental progression of different mutants differed between themselves as well as compared to the wild-type explants. Unfortunately, no reacting *pin1a* explants were found in the examined sample during the CIM response. The wild-type and *pin1b* explants were the most developed at this stage, with visible proliferative bulges developed on the scutellum. These bulges consisted of an epidermal layer of small and compact epidermal cells heavily colored in blue, suggesting a high protein content which points to a high metabolic activity, possibly due to preparations for divisions. Underneath those cells were slightly larger cells still strongly colored blue but also containing pink starch granules. The tissues underneath the proliferative bulges themselves consisted of large starch-rich cells, seemingly vacuolated and containing clearly visible pink starch granules. The *pin1a* × *pin1b* explant cross-section revealed the same cell types, although the proliferative bulges there did not reach the same stage and were not evidently protruding from the scutellum. Based on conclusion presented in Wehbi et al. (2022), these solely blue epidermal cells are the ones undergoing division. The role of these two layers underneath cannot be elucidated with confidence in this manner, but considering their starch content as well as the physiological role of the scutellum tissue they belong to, a role in storage and transport of nutrients could be suggested. One thing to stress is that the origin of the tissues building the proliferative bulge is unclear. Wehbi et al. (2022) detected cell divisions at D3<sub>CIM</sub> in the epidermis but this does not exclude the subepidermal layer as a tissue of origin of the proliferative bulges.

In explants at D3<sub>SIM</sub>, the development of proliferative bulges into proembryogenic masses could be seen, with the developmental progression of different mutants again differing between themselves as well as when compared to the wild-type explant. Again, the wild-type explant exhibited best potential for SE with a well-developed early somatic embryo detected

along with abundant proembryogenic masses. Explants of *pin1a*, *pin1b* and *pin1a* × *pin1b* mutants fared similarly, with just proembryogenic masses present in all. The masses are still connected with the scutellum although it is questionable how functional that link is considering that the cell of the scutellum appear to be in a state of decay. Three groups of cell layers appear to be present in all explants. The epidermal cell layer, the underlying subepidermal tissue and spots of dense cell masses inside the subepidermis. The nature and function of these cells cannot be determined, but perhaps on the basis of their similarity to adult meristematic cells that stain similarly, they could represent a proembryogenic mass with a visible protoderm and future meristems developing inside, as reported in Wehbi et al. (2022).

All in all, histological comparisons did not significantly further the understanding of functions of explored PIN transporters but pointed to a difference in response to SE induction. Although this experiment was preliminary so the response in various explants was not quantified, when taking into consideration the number of explants found to respond favorably to SE, wild-type explants come first, followed by *pin1b* and *pin1a* × *pin1b* and with *pin1a* last. This is interesting to compare to results presented in Wehbi (2020), where the response of the same loss-of-function mutants to embryogenic callus production is explored. Wehbi confirmed that *pin1a* mutants produce such callus better than the *pin1b*, *pin1a* × *pin1b* and the wild-type explants. Taking into consideration findings of O'Connor et al. (2014) on PIN1a function in transforming broad regions of polar auxin flux into narrow canals and the overarching presence of PIN1a during SE presented in this work, its importance in SE becomes even more evident. I hypothesize that *pin1a* mutants excel in callus production due to the lack of auxin canalization that results in broad auxin presence which induces cellular proliferation. On the other hand, the overarching presence of PIN1a during SE points to an unknown function that could be essential in SE, as witnessed by the lowered response to induction in *pin1a* mutants. Of course, this hypothesis needs to be directly investigated as the current data only point to such a possibility, with no quantitative studies on somatic embryo production for the examined mutants available. Even if PIN1a is found to be essential for sEMB production, the question still remains as to why *pin1a* mutants still produce sEMBs and whether this could be attributed to general functional redundancy in functioning of PIN transporters.

In conclusion, this exploratory experiment revealed no cellular differences across the mutants and the wild-type explant, but it did reveal the existence of a difference in response of the *pin1a*, *pin1b* and *pin1a* × *pin1b* mutants compared to the wild-type. To be more exact, the mutants exhibit a delay in response to SE. As the experiment was preliminary and

done on a small sample, physiological differences between the explants cannot be excluded as a reason for this. An open question that remains still is, whether the mutants would eventually develop to the same extent as the wild-type explant, only after a longer time period. Another unknown that was not explored is whether these mutants will give rise to true-to-type plants after regeneration. Overall, further experiments should focus on quantification on a representative sample and analyze the explants at stages of responding embryos, temporal aspect of their development and ultimately, their ability to regenerate to adult plants.

### 5.5 Proposed hypothetical model of developmental events occurring during somatic embryogenesis of *B. distachyon*

Based on the interpretations of presented results, a hypothetical sequence of events taking place during SE in *B. distachyon* can be postulated. Hypothetically, SE is first initiated either directly by 2,4-D or by its effect on internal auxin levels in an area of the scutellum opposite the coleorhiza, a dorsal part of the zEMB where a fountain-like vascular structure is located (Wehbi 2020). Wehbi theorizes that the significance of this area lays in either the presence of perivascular pluripotent cells that are a source of the dividing cells or that the presence of the vasculature allows for a polar flux of auxin to be established which in part switches certain cells on the path of somatic embryogenesis.

Whatever the source of these cells is, formation of local auxin maxima brings about the initiation of SE as early as D2<sub>CIM</sub>. I propose that this maximum is formed with endogenous auxin synthesized by the cells that incited to produce it by 2,4-D. I propose this occurs as a consequence of SoPIN1 activity, for which it was determined that it forms auxin convergence points in the epidermis of developing shoot meristems of *B. distachyon* (O'Connor et al. 2014). PIN1a could also be involved in creation of convergence points due to its wide expression pattern but this is hard to conclude as the correlation with PIN1a and auxin trackers in real time could not be established with the available *Brachypodium* lines. Following initiation, proliferative bulges form and grow, indicating the occurrence of the induction stage of SE. This starts at D3<sub>CIM</sub> and lasts to sometimes before D3<sub>SIM</sub> stage is reached. I would propose that during this phase, the canalization activity of PIN1b is sequestering auxin from the proliferative bulges to the underlying and surrounding tissues of the scutellum. This is supported by findings of DR5-driven RFP expression. With SoPIN1 organizing auxin maxima epidermally, PIN1b could be the one channeling the flow inwards and away. PIN1a could again potentially be involved

in efflux of auxin, driving it from the epidermal cells along with SoPIN1, although I base this suggestion on PIN1a's hypothetical function and its distribution in the epidermal layer that resembles concentration-based PIN distributions models of auxin flux.

Continuing on, sometimes between D2<sub>SIM</sub> and D3<sub>SIM</sub> the developing somatic embryos become separated from the mother-tissue they arose from, entering the maturation phase of SE. Before this separation occurs, I suspect that the three examined PINs still drive auxin flow outwards from the embryogenic masses in the same manner that is hypothetically suggested to develop at D3<sub>CIM</sub>, ceasing with the siphoning at the moment when sEMBs vasculature becomes separated. Arriving to D3<sub>SIM</sub>, some parts of the explant already contain sEMBs with discernible mature zygotic tissues. It would seem that the explored PINs take up their physiological functions starting from this point, but what these functions are and how the PINs are distributed in a developed embryo was not explored as a part of this study.

Important to bear in mind is how this hypothesis relies heavily on PIN1a, PIN1b and SoPIN1 functions analyzed by O'Connor et al. (2014) and O'Connor et al. (2017) and the presumption that their function remains the same both in initiation of spikelets in the shoot meristem and sEMB formation. Even though the histological distribution patterns of the PINs differ during these two processes, they are still developmentally active, albeit under considerably different physiological circumstances. Due to this, the question remains whether these PINs are regulated and function the same in both situations although findings point to that their function is possibly conserved in different developmental processes (Hao et al. 2021). The hypothetical sequence of events presented is also built upon on publications of Wehbi (2020) and Wehbi et al. (2022). On the other hand, the differing distribution patterns of PIN1a during SE and spikelet initiation create doubt whether such interpolations hold true.

Additional uncertainty that marks my hypothesis is whether SE can be grouped together with developmental programs of organogenesis that were suggested to share the same mode of initiation by Benkova et al. (2003). Exploring the development of various organs from meristematic tissues of *A. thaliana*, they identify a convergence of auxin in epidermal cells and its efflux towards tissues underneath as an initiation signal for development. Yet an important difference between physiological organogenesis and SE is that sEMBs eventually develop their own vasculature and become independent of the mother-tissue. Thus, an additional event must occur through which they gain this independence. How this occurs during SE of *B. distachyon*, remains unknown.

One important point that challenges this hypothesis is how to reconcile the occurrence of the purported auxin flux in proliferative bulges, driven by presence action of epidermally present PIN1a and SoPIN1, after their formation. DR5-driven transcription of RFP slows down after initiation of SE and the growing bulges exhibit less and less RFP. This points to a drop in auxin-related transcription. But for the flux to remain, auxin needs to be synthesized in these cells. Perhaps a high concentration of PIN transporters does not allow intracellular auxin to act on the cells it is produced in. Supporting this is the distribution of VENUS at D3<sub>CIM</sub>, which marks strongly the epidermal layer and is absent both in the rest of the bulge and the tissues surrounding them. I suspect that auxin is siphoned through the cell with such a high turnover that it does not affect VENUS degradation either. How does auxin turnover rate relate to auxin-related degradation has not been explored previously, so no firm conclusions can be made. This question is also relevant for the SIM phase of induction as PIN1a's and SoPIN1's distribution patterns do not change drastically. Unfortunately, no data on response of the DII-VENUS marker to SIM is available. However, in an examination of zygotic development of *B. distachyon* also utilizing the DR5 driven transcription of RFP, no response was found during the earliest stages of embryogenesis (Hao et al. 2021) which goes to show that auxin-related transcription potentially does not occur at that point.

Evidently, there is much left to examine before the process of SE in *B. distachyon* can be described properly. An unanswered question is the response of DII-VENUS marker during SIM which I was not able to examine due to technical difficulties. Perhaps the most important remaining question is the origin of cells that give rise to somatic embryos as no events that shed light on this have been observed. Presented findings point to an epidermal origin but it is not clear whether proliferative bulges arise from one or from a cluster of cells. The way forward in research of this topic would be examining the histological events of SE occurring in *B. distachyon* on a cellular scale, to clearly determine the flow of auxin through the revelation of cellular polar distribution of the fluorescently-tagged PIN proteins. Particular interest should be given to developmental changes occurring around D2<sub>CIM</sub> as that is when first divisions start. Other than microscopy methods, techniques such as transcriptomic profiling utilizing Next Generation Sequencing could reveal cellular populations that belong to same developmental lineages through identification of commonly expressed transcriptomic patterns. In conclusion, the synthesis of observed events into the interpretation of SE occurring in *B. distachyon* I present here opens a way for future improvements in our understanding of these fascinating developmental events.

## 6. CONCLUSION

---

Examination of distribution patterns of selected PIN auxin transporters of *B. distachyon* (PIN1a, PIN1b and SoPIN1) along with detection of auxin with the use of transcriptional and degron-based markers during early stages of SE were carried out utilizing confocal microscopy. Results of this approach shed light upon the events occurring during the initiation and induction stage of SE along with highlighting to a certain extent the effect of auxin flux, shaped by the observed PIN transporters.

PIN1a is present throughout occurrence of SE, initially marking area of the scutellum where proliferative bulges appear and grow. Its pattern of distribution evolves to strongly mark plasma membranes in growing proliferative bulges where epidermal cells touch each other and the first underlying layer. I suggest this points to their function in siphoning auxin from these cells towards the inner tissues of the bulge. Unfortunately, such an assumption could not be backed by data on auxin presence measured with auxin trackers.

As PIN1b and SoPIN1 were observed in conjunction and in the same line that also contained a DR5-based transcriptional reporter of auxin, correlation of auxin presence and PIN distribution could be established. With SoPIN1 and PIN1b first mostly overlapping in expression in the scutellum where SE is expected to occur, soon their patterns start to diverge, with SoPIN1 associating with the epidermal layer and PIN1b with the inner tissues below. Taking into notice a spike in the epidermal layer of the scutellum of the DR5-driven RFP expression that is followed by the split in the two PINs expression zones, I propose that through activity of SoPIN1, SE is initiated through a creation of an auxin maximum in the scutellum epidermis. The initiation results in appearance of proliferative bulges in which flux of auxin flows from the epidermis and through the inner tissues. I suggest that SoPIN1 plays a role in siphoning auxin to inner tissues of a bulge, as it is displayed in membranes of epidermal cells in contact between each other and with the first underlying layer below. As for the role of PIN1b, its nonpolarized presence in the inner tissues suggests that it channels auxin driven away from the epidermis to the tissue of the scutellum. I suspect that this channeling of auxin results in a lack of DR5-driven RFP expression in growing proliferative bulges.

Observation of the DII-VENUS degron-based marker of auxin presence supports these findings albeit an interesting pattern of its presence is noted during growth of proliferative bulges. Being constitutively expressed, VENUS is initially present globally but fades with prolonged contact of the explant with auxin. After proliferative bulges have formed, VENUS



is visible solely in their epidermis, neither in the inside of the bulges or in the surrounding scutellum. I suspect this pattern is due to channeling of endogenous auxin from the epidermal layer to the inner tissues and beyond with such a turnover that VENUS is not degraded.

Additionally, no histological differences observable using PAS/NBB staining between *pin1a*, *pin1b* and *pin1a* × *pin1b* mutants in comparison to a wild-type explant were detected so presumably, SE still occurs owing to the other PIN transporters taking on the functions of the missing ones. Nevertheless, a delay in response to SE was detected in the mutant lines when compared to the wild-type. This finding opens up future avenues of research that could lead to functional characterization of the studied PIN transporters.

## 7. REFERENCES

---

- Atta, R., Laurens, L., Boucheron-Dubuisson, E., Guivarc'h, A., Carnero, E., Giraudat-Pautot, V., Rech, P., & Chriqui, D. (2009). Pluripotency of Arabidopsis xylem pericycle underlies shoot regeneration from root and hypocotyl explants grown *in vitro*. *The Plant Journal*, *57*(4), 626–644.
- Barciszewski J, Rattan S. I. S., Siboska G., Clark B. F. C. (1999). Kinetin – 45 years on. *Plant Science* *148*, 37 – 45.
- Benková, E., Michniewicz, M., Sauer, M., Teichmann, T., Seifertová, D., Jürgens, G., & Friml, J. (2003). Local, Efflux-Dependent Auxin Gradients as a Common Module for Plant Organ Formation. *Cell*, *115*(5), 591–602.
- Betekhtin, A., Hus, K., Rojek-Jelonek, M., Kurczynska, E., Nibau, C., Doonan, J. H., & Hasterok, R. (2020). In Vitro Tissue Culture in Brachypodium: Applications and Challenges. *International Journal of Molecular Sciences*, *21*(3), 1037.
- Bhatla S. C. (2018). Auxins. In: Bhatla, S. C., & A. Lal, M. (2018). *Plant Physiology, Development and Metabolism*, Springer Singapore, pp. 569 – 601.
- Boer, D. R., Freire-Rios, A., van den Berg, W. A. M., Saaki, T., Manfield, I. W., Kepinski, S., López-Vidriero, I., Franco-Zorrilla, J. M., de Vries, S. C., Solano, R., Weijers, D., & Coll, M. (2014). Structural Basis for DNA Binding Specificity by the Auxin-Dependent ARF Transcription Factors. *Cell*, *156*(3), 577–589.
- Bragg, J. N., Anderton, A., Nieu, R., & Vogel, J. P. (2015). Brachypodium distachyon. In K. Wang (Ed.) (2015). *Agrobacterium Protocols* (Vol. 1223), Springer New York, pp. 17–33.
- Brunoud, G., Wells, D. M., Oliva, M., Larrieu, A., Mirabet, V., Burrow, A. H., Beeckman, T., Kepinski, S., Traas, J., Bennett, M. J., & Vernoux, T. (2012). A novel sensor to map auxin response and distribution at high spatio-temporal resolution. *Nature*, *482*(7383), 103–106.
- Brkljacic, J., Grotewold, E., Scholl, R., Mockler, T., Garvin, D. F., Vain, P., Brutnell, T., Sibout, R., Bevan, M., Budak, H., Caicedo, A. L., Gao, C., Gu, Y., Hazen, S. P., Holt, B. F., Hong, S.-Y., Jordan, M., Manzaneda, A. J., Mitchell-Olds, T., et al., Vogel, J. P. (2011). Brachypodium as a Model for the Grasses: Today and the Future. *Plant Physiology*, *157*(1), 3–13.
- Draper, J., Mur, L. A. J., Jenkins, G., Ghosh-Biswas, G. C., Bablak, P., Hasterok, R., & Routledge, A. P. M. (2001). *Zeadistachyon*. A New Model System for Functional Genomics in Grasses. *Plant Physiology*, *127*(4), 1539–1555.

- Elhiti, M., Stasolla, C. (2022). Transduction of Signals during Somatic Embryogenesis. *Plants*, *11*(2), 178.
- Elhiti, M., Tahir, M., Gulden, R. H., Khamiss, K., & Stasolla, C. (2010). Modulation of embryo-forming capacity in culture through the expression of Brassica genes involved in the regulation of the shoot apical meristem. *Journal of Experimental Botany*, *61*(14), 4069–4085.
- Enders, T. A., & Strader, L. C. (2015). Auxin activity: Past, present, and future. *American Journal of Botany*, *102*(2), 180–196.
- Fehér, A. (2015). Somatic embryogenesis—Stress-induced remodeling of plant cell fate. *Biochimica et Biophysica Acta (BBA) - Gene Regulatory Mechanisms*, *1849*(4), 385–402.
- Forestan, C., Farinati, S., & Varotto, S. (2012). The Maize PIN Gene Family of Auxin Transporters. *Frontiers in Plant Science*, *3*.
- Forestan, C., Meda, S., & Varotto, S. (2010). ZmPIN1-Mediated Auxin Transport Is Related to Cellular Differentiation during Maize Embryogenesis and Endosperm Development. *Plant Physiology*, *152*(3), 1373–1390.
- Gaj, M. D. (2004). Factors Influencing Somatic Embryogenesis Induction and Plant Regeneration with Particular Reference to *Arabidopsis thaliana* (L.) Heynh. *Plant Growth Regulation*, *43*(1), 27–47.
- Garrocho-Villegas V., de Jesús-Olivera M. T., Quintanar E. S. (2012). Maize Somatic Embryogenesis: Recent Features to Improve Plant Regeneration. In: Loyola-Vargas, V. M., & Ochoa-Alejo, N. (Eds.). (2012). *Plant Cell Culture Protocols* (Vol. 877), Humana Press, pp. 173 – 182.
- Geisler, M., Aryal, B., di Donato, M., & Hao, P. (2017). A Critical View on ABC Transporters and Their Interacting Partners in Auxin Transport. *Plant and Cell Physiology*, *58*(10), 1601–1614.
- Girin, T., David, L. C., Chardin, C., Sibout, R., Krapp, A., Ferrario-Méry, S., & Daniel-Vedele, F. (2014). Brachypodium: A promising hub between model species and cereals. *Journal of Experimental Botany*, *65*(19), 5683–5696.
- Gottlieb, A., Müller, H.-G., Massa, A. N., Wanjugi, H., Deal, K. R., You, F. M., Xu, X., Gu, Y. Q., Luo, M.-C., Anderson, O. D., Chan, A. P., Rabinowicz, P., Devos, K. M., & Dvorak, J. (2013). Insular Organization of Gene Space in Grass Genomes. *PLoS ONE*, *8*(1), e54101.
- Hagen, G., Martin, G., Li, Y., & Guilfoyle, T. J. (1991). Auxin-induced expression of the soybean GH3 promoter in transgenic tobacco plants. *Plant Molecular Biology*, *17*(3), 567–579.

- Hao, Z., Zhang, Z., Xiang, D., Venglat, P., Chen, J., Gao, P., Datla, R., & Weijers, D. (2021). Conserved, divergent and heterochronic gene expression during *Brachypodium* and *Arabidopsis* embryo development. *Plant Reproduction*, *34*(3), 207–224.
- Horstman, A., Bemer, M., & Boutilier, K. (2017). A transcriptional view on somatic embryogenesis. *Regeneration*, *4*(4), 201–216.
- Jedličková V., Naghani S. E., Robert H. S. (2022). On the trail of auxin: Reporters and sensors. *Plant Cell*, *34*(9), 3200-3213.
- Jin, F., Hu, L., Yuan, D., Xu, J., Gao, W., He, L., Yang, X., & Zhang, X. (2014). Comparative transcriptome analysis between somatic embryos (SEs) and zygotic embryos in cotton: Evidence for stress response functions in SE development. *Plant Biotechnology Journal*, *12*(2), 161–173.
- Joint Genome Institute (n.d.). Phytozome. *U.S. Department of Energy*, accessed 30 november 2022 (<https://phytozome.jgi.doe.gov/pz/portal.html>)
- Křeček, P., Skůpa, P., Libus, J., Naramoto, S., Tejos, R., Friml, J., & Zažímalová, E. (2009). The PIN-FORMED (PIN) protein family of auxin transporters. *Genome Biology*, *10*(12), 249.
- Kurihara, D., Mizuta, Y., Sato, Y., & Higashiyama, T. (2015). ClearSee: A rapid optical clearing reagent for whole-plant fluorescence imaging. *Development*, *142*(23), 4168–4179.
- Kutschera, U., & Ray, P. M. (2022). Forever young: Stem cell and plant regeneration one century after Haberlandt 1921. *Protoplasma*, *259*(1), 3–18.
- Leljak-Levanić, D., Mihaljević, S., & Bauer, N. (2015). Somatic and zygotic embryos share common developmental features at the onset of plant embryogenesis. *Acta Physiologiae Plantarum*, *37*(7), 127.
- Leyser, O. (2011). Auxin, Self-Organisation, and the Colonial Nature of Plants. *Current Biology*, *21*(9), R331–R337.
- Li, S.-B., Xie, Z.-Z., Hu, C.-G., & Zhang, J.-Z. (2016). A Review of Auxin Response Factors (ARFs) in Plants. *Frontiers in Plant Science*, *7*.
- Liao, C.-Y., Smet, W., Brunoud, G., Yoshida, S., Vernoux, T., & Weijers, D. (2015). Reporters for sensitive and quantitative measurement of auxin response. *Nature Methods*, *12*(3), 207–210.
- Loyola-Vargas, V. M., & Ochoa-Alejo, N. (2016). Somatic embryogenesis. An overview. In: Loyola-Vargas, V. M., & Ochoa-Alejo, N. (Eds.). (2016). *Somatic Embryogenesis: Fundamental Aspects and Applications*, Springer International Publishing, pp. 1 – 8.

- Martinez, C. C., Koenig, D., Chitwood, D. H., & Sinha, N. R. (2016). A sister of PIN1 gene in tomato (*Solanum lycopersicum*) defines leaf and flower organ initiation patterns by maintaining epidermal auxin flux. *Developmental Biology*, 419(1), 85–98.
- Mayer, K. F. X., Martis, M., Hedley, P. E., Šimková, H., Liu, H., Morris, J. A., Steuernagel, B., Taudien, S., Roessner, S., Gundlach, H., Kubaláková, M., Suchánková, P., Murat, F., Felder, M., Nussbaumer, T., Graner, A., Salse, J., Endo, T., Sakai, H., Itoh, T., Sato, K., Platzer, M., Matsumoto, T., Scholz, U., Doležel, J., Waugh, R., Stein, N. (2011). Unlocking the Barley Genome by Chromosomal and Comparative Genomics. *The Plant Cell*, 23(4), 1249–1263.
- Miller C.O., Skoog F., von Saltza M.H., Strong F.M. (1955). Kinetin, a cell division factor from deoxyribonucleic acid. *Journal of the American Chemical Society*, 77, 1392.
- Mir, R., Aranda, L. Z., Biaocchi, T., Luo, A., Sylvester, A. W., & Rasmussen, C. G. (2017). A DII Domain-Based Auxin Reporter Uncovers Low Auxin Signaling during Telophase and Early G1. *Plant Physiology*, 173(1), 863–871.
- O'Connor, D. L., Elton, S., Ticchiarelli, F., Hsia, M. M., Vogel, J. P., & Leyser, O. (2017). *Cross-species functional diversity within the PIN auxin efflux protein family*. *eLife* 6:e31804.
- O'Connor, D. L., Runions, A., Sluis, A., Bragg, J., Vogel, J. P., Prusinkiewicz, P., & Hake, S. (2014). A Division in PIN-Mediated Auxin Patterning during Organ Initiation in Grasses. *PLoS Computational Biology*, 10(1), e1003447.
- Ochoa-Alejo, N. (2016). The Uses of Somatic Embryogenesis for Genetic Transformation. In: Loyola-Vargas, V. M., & Ochoa-Alejo, N. (Eds.). (2016). *Somatic Embryogenesis: Fundamental Aspects and Applications*, Springer International Publishing, pp. 415 – 434.
- Oliveira, E. J., Koehler, A. D., Rocha, D. I., Vieira, L. M., Pinheiro, M. V. M., de Matos, E. M., da Cruz, A. C. F., da Silva, T. C. R., Tanaka, F. A. O., Nogueira, F. T. S., & Otoni, W. C. (2017). Morphohistological, histochemical, and molecular evidences related to cellular reprogramming during somatic embryogenesis of the model grass *Brachypodium distachyon*. *Protoplasma*, 254(5), 2017–2034.
- Pacios-Bras, C., Schlaman, H. R. M., Boot, K., Admiraal, P., Mateos Langerak, J., Stougaard, J., & Spaink, H. P. (2003). Auxin distribution in *Lotus japonicus* during root nodule development. *Plant Molecular Biology*, 52(6), 1169–1180.
- Scholthof, K.-B. G., Irigoyen, S., Catalan, P., & Mandadi, K. K. (2018). *Brachypodium*: A Monocot Grass Model Genus for Plant Biology. *The Plant Cell*, 30(8), 1673–1694.
- She, M., Yin, G., Li, J., Li, X., Du, L., Ma, W., & Ye, X. (2013). Efficient Regeneration Potential is Closely Related to Auxin Exposure Time and Catalase Metabolism During the Somatic

- Embryogenesis of Immature Embryos in *Triticum aestivum* L. *Molecular Biotechnology*, 54(2), 451–460.
- Su, Y. H., & Zhang, X. S. (2009). Auxin gradients trigger de novo formation of stem cells during somatic embryogenesis. *Plant Signaling & Behavior*, 4(7), 574–576.
- Sugimoto, K., Gordon, S. P., & Meyerowitz, E. M. (2011). Regeneration in plants and animals: Dedifferentiation, transdifferentiation, or just differentiation? *Trends in Cell Biology*, 21(4), 212–218.
- The International Brachypodium Initiative. (2010). Genome sequencing and analysis of the model grass *Brachypodium distachyon*. *Nature*, 463, 763–768
- van Berkel, K., de Boer, R. J., Scheres, B., & ten Tusscher, K. (2013). Polar auxin transport: Models and mechanisms. *Development*, 140(11), 2253–2268.
- van der Graaff, E., Laux, T., & Rensing, S. A. (2009). The WUS homeobox-containing (WOX) protein family. *Genome Biology*, 10(12), 248.
- Verma, D., Joshi, R., Shukla, A., & Kumar, P. (2011). Protocol for in vitro somatic embryogenesis and regeneration of rice (*Oryza sativa* L.). *Indian journal of experimental biology*, 49(12), 958–963.
- Vieten, A., Vanneste, S., Wiśniewska, J., Benková, E., Benjamins, R., Beeckman, T., Luschnig, C., & Friml, J. (2005). Functional redundancy of PIN proteins is accompanied by auxin-dependent cross-regulation of PIN expression. *Development*, 132(20), 4521–4531.
- Vogel, J., & Hill, T. (2008). High-efficiency *Agrobacterium*-mediated transformation of *Brachypodium distachyon* inbred line Bd21-3. *Plant Cell Reports*, 27(3), 471–478.
- Wang, J.-R., Hu, H., Wang, G.-H., Li, J., Chen, J.-Y., & Wu, P. (2009). Expression of PIN Genes in Rice (*Oryza sativa* L.): Tissue Specificity and Regulation by Hormones. *Molecular Plant*, 2(4), 823–831.
- Wehbi H. (2020): Study of the genetic factors controlling early stages of somatic embryogenesis in *Brachypodium distachyon*. Doctoral thesis, Paris-Saclay University, Doctoral School n°567 Sciences du Végétal, Gif-sur-Yvette.
- Wehbi, H., Soulhat, C., Morin, H., Bendahmane, A., Hilson, P., & Bouchabké-Coussa, O. (2022). One-Week Scutellum Somatic Embryogenesis in the Monocot *Brachypodium distachyon*. *Plants*, 11(8), 1068.
- Williams, E. G., & Maheswaran, G. (1986). Somatic Embryogenesis: Factors Influencing Coordinated Behaviour of Cells as an Embryogenic Group. *Annals of Botany*, 57(4), 443–462.

- Winkelmann, T. (2016). Somatic Versus Zygotic Embryogenesis: Learning from Seeds. In M. A. Germana & M. Lambardi (Eds.). (2016). *In Vitro Embryogenesis in Higher Plants* Vol. 1359, Springer New York, pp. 25–46.
- Wójcikowska B. & Gaj M. D. (2016). Somatic Embryogenesis in Arabidopsis. In: Loyola-Vargas, V. M., & Ochoa-Alejo, N. (Eds.). (2016). *Somatic Embryogenesis: Fundamental Aspects and Applications*, Springer International Publishing, pp. 185–195
- Wójcikowska, B., & Gaj, M. D. (2017). Expression profiling of AUXIN RESPONSE FACTOR genes during somatic embryogenesis induction in Arabidopsis. *Plant Cell Reports*, 36(6), 843–858.
- Wybouw, B., & De Rybel, B. (2019). Cytokinin – A Developing Story. *Trends in Plant Science*, 24(2), 177–185.
- Yang, J., Yuan, Z., Meng, Q., Huang, G., Périn, C., Bureau, C., Meunier, A.-C., Ingouff, M., Bennett, M. J., Liang, W., & Zhang, D. (2017). Dynamic Regulation of Auxin Response during Rice Development Revealed by Newly Established Hormone Biosensor Markers. *Frontiers in Plant Science*, 8.
- Zhou, C., Han, L., Hou, C., Metelli, A., Qi, L., Tadege, M., Mysore, K. S., & Wang, Z.-Y. (2011). Developmental Analysis of a *Medicago truncatula smooth leaf margin1* Mutant Reveals Context-Dependent Effects on Compound Leaf Development. *The Plant Cell*, 23(6), 2106–2124.
- Zhou, J.-J., & Luo, J. (2018). The PIN-FORMED Auxin Efflux Carriers in Plants. *International Journal of Molecular Sciences*, 19(9), 2759.
- Zimmerman J. L., (1993). Somatic Embryogenesis: A Model for Early Development in Higher Plants. *The Plant Cell*, Vol. 5, 1411-1423.

## 8. CURRICULUM VITAE

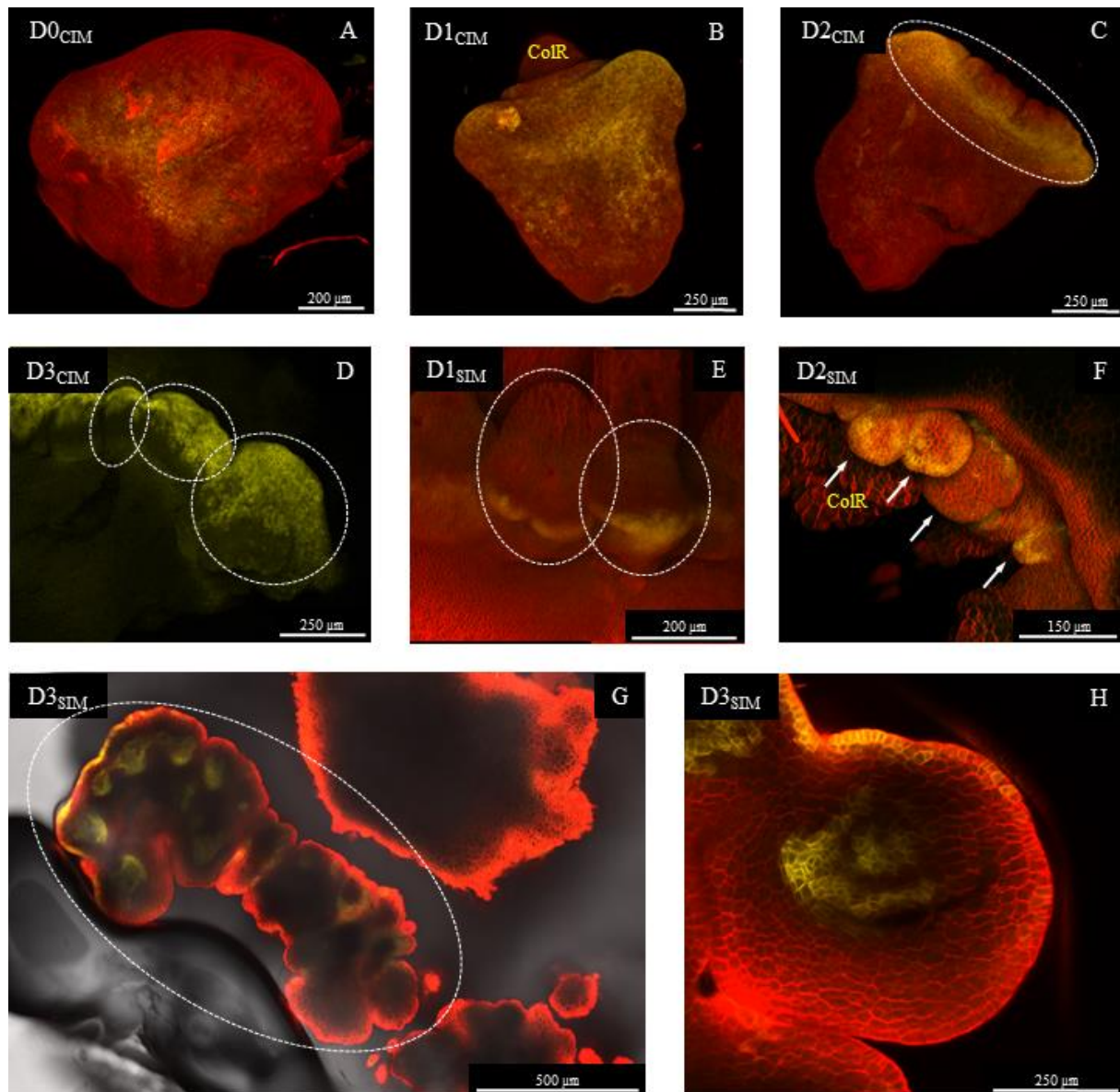
---

I was born in Zagreb, Republic of Croatia, where I attended primary as well as high school. In September 2017, I enrolled in the Undergraduate Program of Molecular Biology at the Faculty of Science, University of Zagreb. After completing it and obtaining the title of Bachelor in Molecular Biology, I continued my studies at the Faculty of Science in Zagreb, enrolling in the Graduate Program of Molecular Biology in September 2020 and completing it in 2022, earning the title of Master in Molecular Biology. During my time at the Faculty of Science in Zagreb, I took part in two separate internships at the Department of Zoology and one internship in the Laboratory for Molecular Genetics at Ruđer Bošković Institute. I spent the final semester of my graduate year at Institut Jean-Pierre Bourgin in Versailles with the aim of doing my master thesis internship in the laboratory of the Cell Biology and Plant Regeneration research team. In addition to this, I was also active in the Biology Student Association “BIUS” and involved in leading the group for studying birds. My working experience as a student is mostly tied to the workplace of an educator in the Zoological park of Zagreb. I am proficient in usage of English and have basic comprehension and communication abilities in French.



## 9. APPENDIX

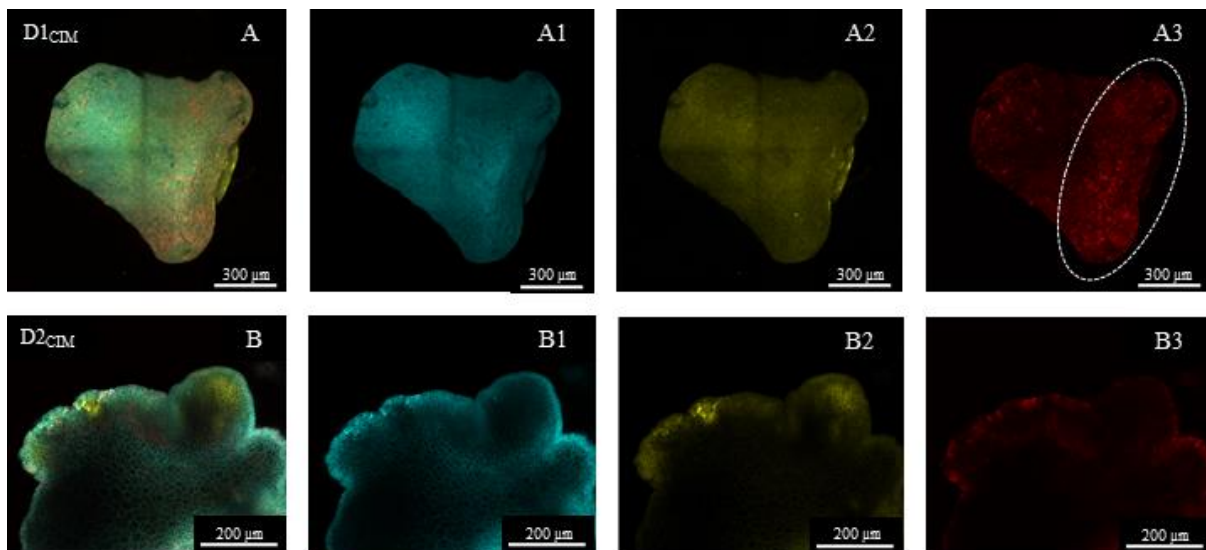
### 9.1 Distribution of PIN1a during somatic embryogenesis



**Supplemental Figure 1. Distribution patterns of PIN1a-Citrine during consecutive days of somatic embryogenesis.** PIN1a-Citrine signal is represented in yellow and the red signal represents the cell walls colored with Calcofluor White. (A) Maximum intensity projection of signal present in the scutellum area at D0<sub>CIM</sub>. (B) Maximum intensity projection of signal present in the scutellum area at D1<sub>CIM</sub>. (C) Maximum intensity projection of signal present in the scutellum area at D2<sub>CIM</sub>. White dotted circle marks the proliferative bulges forming. (D) Maximum intensity projection of signal present in the proliferative bulges at D3<sub>CIM</sub>. Dotted circles mark individual proliferative bulges. (E) Maximum intensity projection of signal present in the proliferative bulges at D1<sub>SIM</sub>. Dotted circles mark some of the individual proliferative bulges. (F) Maximum intensity projection of signal *Continued*

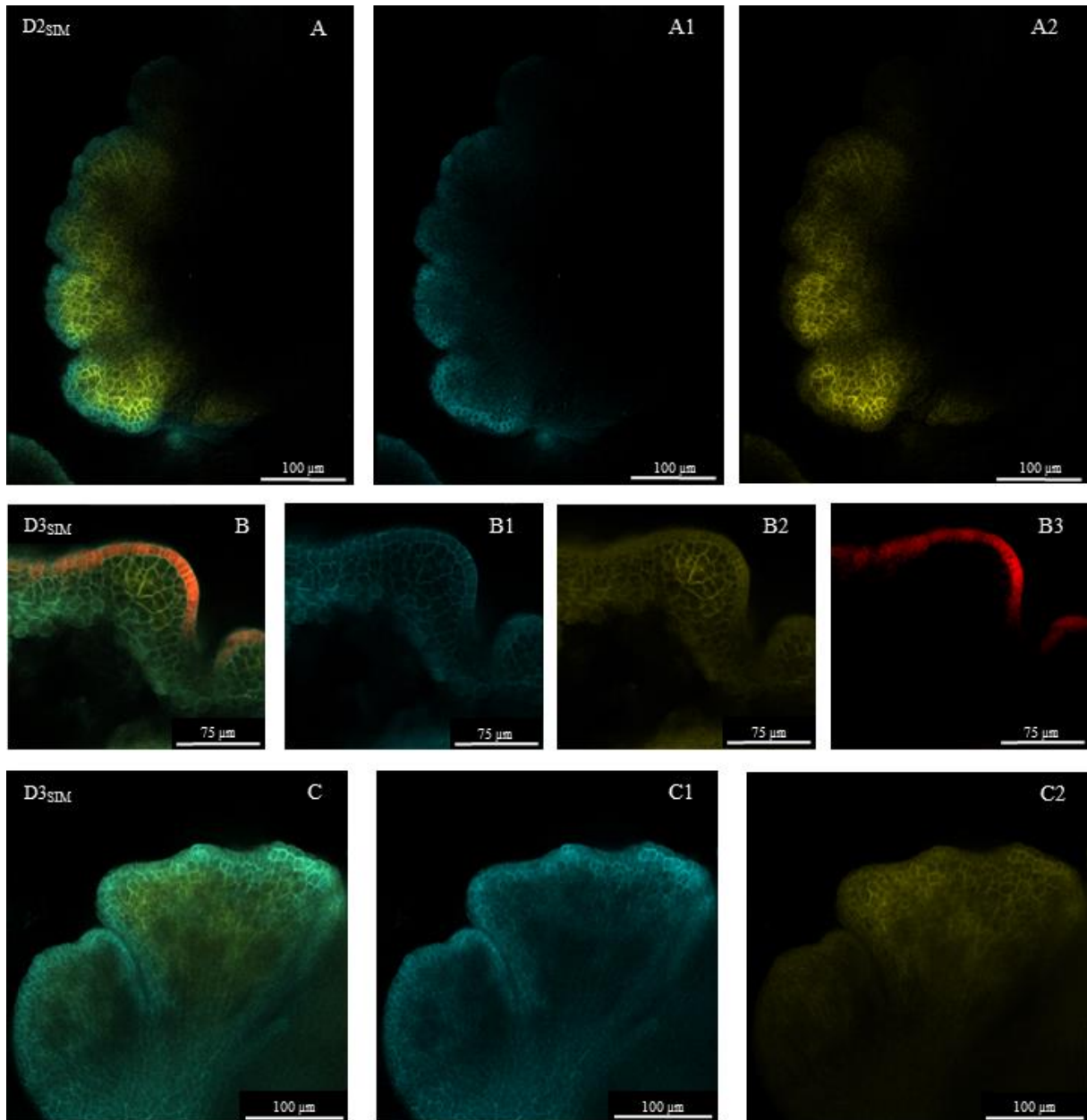
on next page present in the proliferative bulges at D2<sub>SIM</sub>. Arrows mark individual bulges. **(G)** Confocal cross-section of the scutellum at D3<sub>SIM</sub>. Dotted circle marks the large proliferative bulge containing developing somatic embryos. **(H)** Confocal cross-section of a developing root meristem arising from a proliferative bulge at D3<sub>SIM</sub> and exhibiting a developing root cap and root apical meristem. *Abbreviations: D0<sub>CIM</sub> – D3<sub>CIM</sub> and D1<sub>SIM</sub> – D3<sub>SIM</sub> signify the length in days of consecutive explant incubation on callus- and shoot-inducing medium.*

## 9.2 Distribution of PIN1b, SoPIN1 and the transcriptional response to auxin during somatic embryogenesis



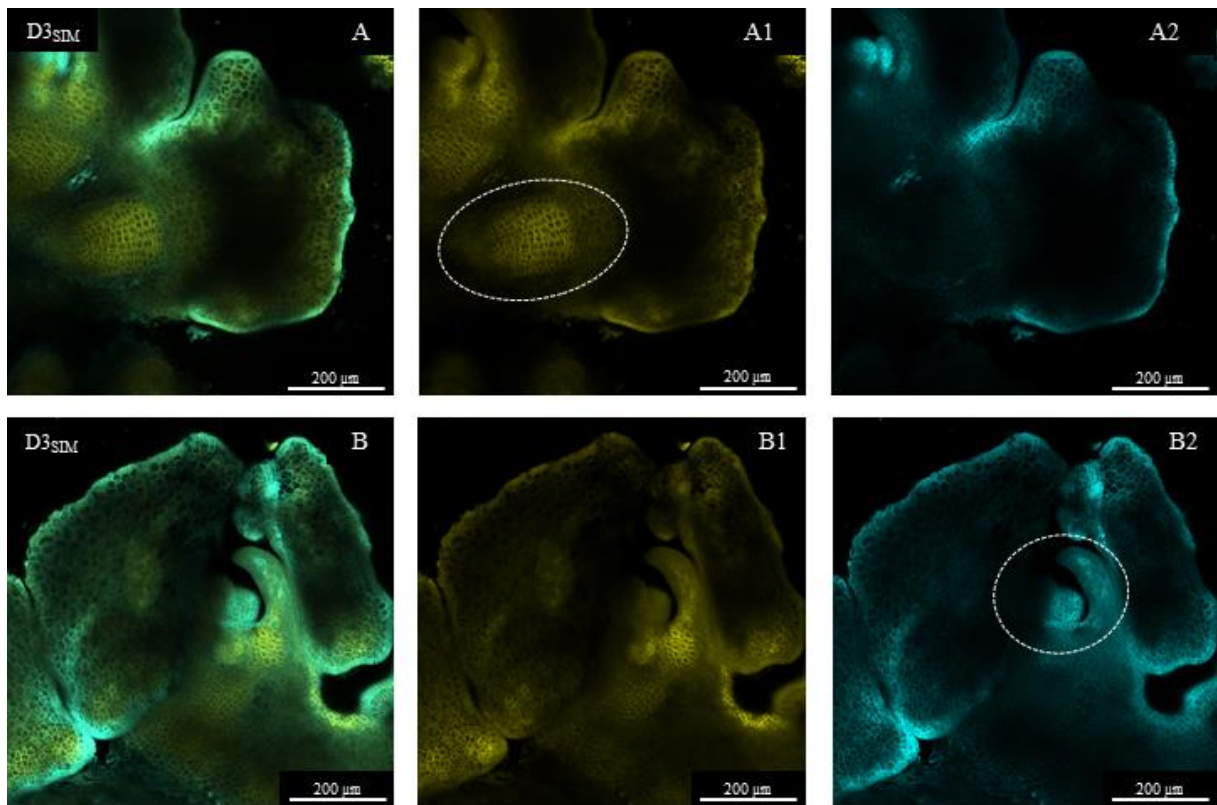
### **Supplemental Figure 2. Distribution patterns of SoPIN1-Cerulean, PIN1b-Citrine presence of auxin tracked by DR5 transcriptional reporter during somatic embryogenesis.**

First image of the series exhibits the overlay of the individual signal distributions throughout the same object. *BdSoPIN1-Cerulean* is shown in blue, *BdPIN1b-Citrine* in yellow and RFP expressed due to auxin presence in red. **(A, A1, A2)** Maximum intensity projection of signal presence in the scutellum at D1<sub>CIM</sub>. **(A3)** Dotted circle marks the area where higher density of RFP is observed. **(B, B1, B2, B3.)** Confocal cross-section of a broader area where formation of proliferative bulges is taking place at D2<sub>CIM</sub>. *Abbreviations: D0<sub>CIM</sub> – D3<sub>CIM</sub> and D1<sub>SIM</sub> – D3<sub>SIM</sub> signify the length in day of consecutive explant incubation on callus- and shoot-inducing medium.*



**Supplemental Figure 3. Distribution patterns of SoPIN1-Cerulean, PIN1b-Citrine presence of auxin tracked by DR5 transcriptional reporter during somatic embryogenesis.**

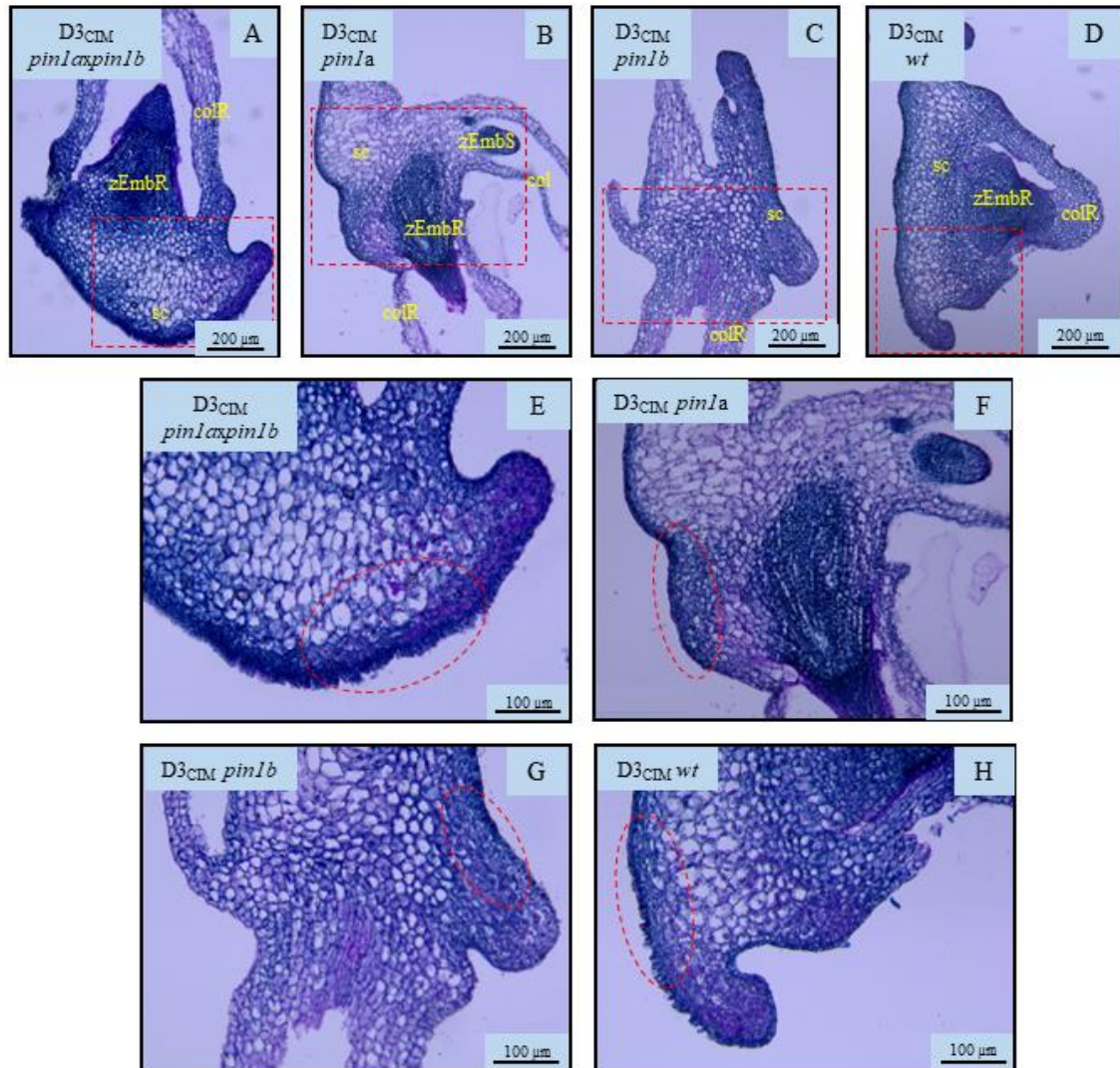
First image of the series exhibits the overlay of the individual signal distributions throughout the same object. *BdSoPIN1-Cerulean* is shown in blue, *BdPIN1b-Citrine* in yellow and RFP expressed due to auxin presence in red. (A, A1, A2) Confocal cross-section of a developmentally progressed proliferative bulge at D2<sub>SIM</sub>. (B, B1, B2, B3) Confocal cross-section of an early developing proliferative bulge at D3<sub>SIM</sub>. (C, C1, C2) Confocal cross-section of a developing proliferative bulge at D3<sub>SIM</sub>. *Abbreviations: D0<sub>CIM</sub> – D3<sub>CIM</sub> and D1<sub>SIM</sub> – D3<sub>SIM</sub> signify the length in days of consecutive explant incubation on callus- and shoot-inducing medium.*



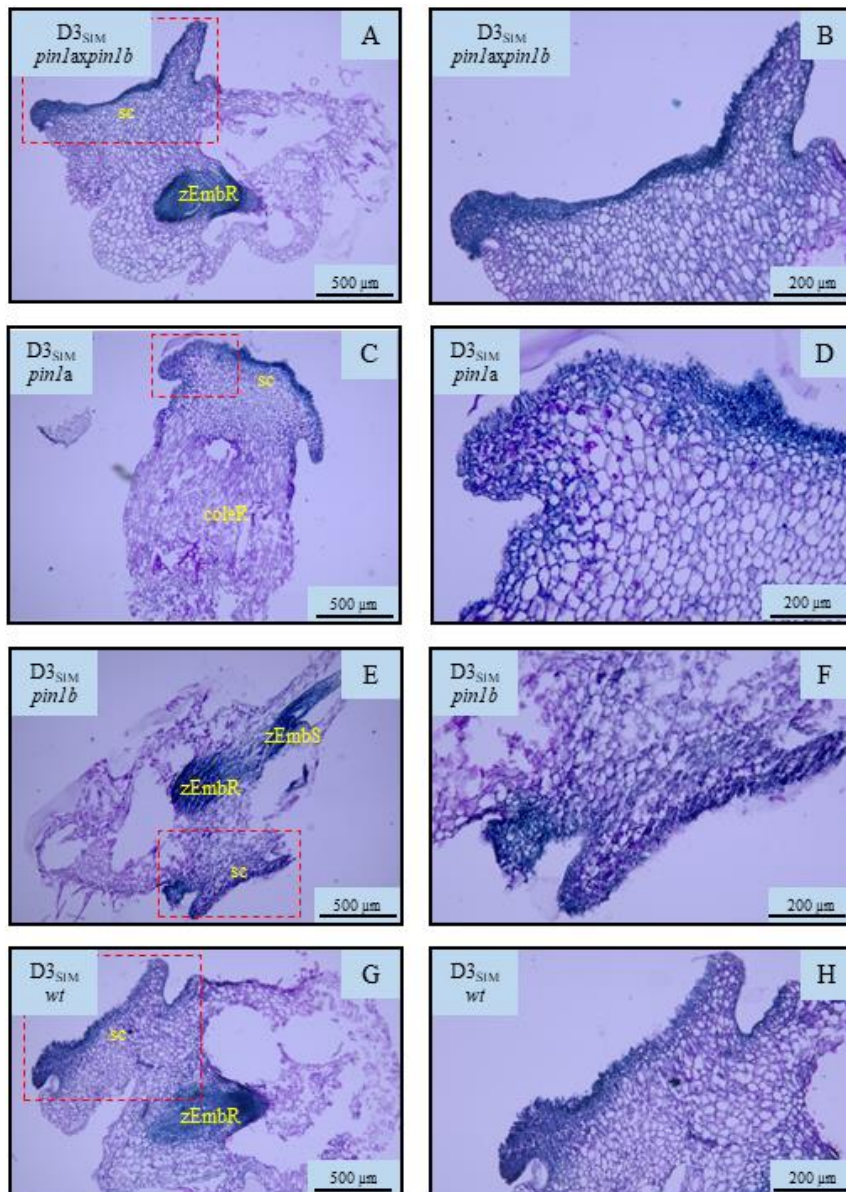
**Supplemental Figure 4. Distribution patterns of SoPIN1-Cerulean, PIN1b-Citrine during somatic embryogenesis.** First image of the series exhibits the overlay of the individual signal distributions throughout the same object. *BdSoPIN1-Cerulean* is shown in blue and *BdPIN1b-Citrine* in yellow. **(A, A1, A2)** Confocal cross-section of a root embryonic tissue protruding from a proliferative bulge at D3<sub>SIM</sub>. **(A1)** Dotted circle marks the root stele. **(B, B1, B2)** Confocal cross-section of a developing embryonic shoot protruding from a proliferative bulge at D3<sub>SIM</sub>. **(B2)** Dotted circle marks the shoot apical meristem. *Abbreviations: D0<sub>CIM</sub> – D3<sub>CIM</sub> and D1<sub>SIM</sub> – D3<sub>SIM</sub> signify the length in days of consecutive explant incubation on callus- and shoot-inducing medium.*



### 9.3 Comparison of tissue sections of *B. distachyon* *pin* loss-of-function mutant explants not responding to somatic embryogenesis



**Supplemental Figure 5. Histological patterns in the *pin1a* x *pin1b*, *pin1a* and *pin1b* loss-of-function mutants in comparison to a wild-type explant at D3<sub>CIM</sub>.** Naphtol Blue Black dyes proteins in blue and cell nuclei in dark blue while Periodic Acid Schiff dyes polysaccharides in pink. (A, D) Transversal cross-section of zygotic embryos. (B, C) Sagittal cross-sections of zygotic embryos. (E, F, G, H) Close-ups of the respective cross-sections A, B, C and D revealing cellular structure of scutellum tissues. Abbreviations: D0<sub>CIM</sub> – D3<sub>CIM</sub> and D1<sub>SIM</sub> – D3<sub>SIM</sub> signify the length in days of consecutive explant incubation on callus- and shoot-inducing medium. sc – scutellum, zEmbR – zygotic embryo root, colR – coleorhiza, zEmbS – zygotic embryo shoot, col – coleoptile



**Supplemental Figure 6. Histological patterns in the *pin1a* x *pin1b*, *pin1a* and *pin1b* loss-of-function mutants in comparison to a wild-type explant at D3<sub>SIM</sub>.** Naphtol Blue Black dyes proteins in blue and cell nuclei in dark blue while Periodic Acid Schiff dyes polysaccharides in pink. (A, C, D) Sagittal cross-sections of zygotic embryos. (B) Transverse cross-section of a zygotic embryo. (E, F, G, H) Close-ups of the respective cross-sections A, B, C and D revealing cellular structure of scutellum tissues. Abbreviations: D0<sub>CIM</sub> – D3<sub>CIM</sub> and D1<sub>SIM</sub> – D3<sub>SIM</sub> signify the length in days of consecutive explant incubation on callus- and shoot-inducing medium. sc – scutellum, zEmbR – zygotic embryo root, colR – coleorhiza, zEmbS – zygotic embryo shoot.